



Idiosyncratic neural coding and neuromodulation of olfactory individuality in *Drosophila*

Kyle S. Honegger^{a,b,1}, Matthew A.-Y. Smith^{a,1}, Matthew A. Churgin^a, Glenn C. Turner^c, and Benjamin L. de Bivort^{a,2}

^aDepartment of Organismic and Evolutionary Biology and Center for Brain Science, Harvard University, Cambridge, MA 02138; ^bComputational Informatics and Visualization Laboratory, Ann & Robert H. Lurie Children's Hospital of Chicago, Chicago, IL 60611; and ^cJanelia Research Campus, Howard Hughes Medical Institute, Ashburn, VA 20147

Edited by Marla B. Sokolowski, University of Toronto, Toronto, Canada, and accepted by Editorial Board Member Gene E. Robinson July 30, 2019 (received for review March 8, 2019)

Innate behavioral biases and preferences can vary significantly among individuals of the same genotype. Though individuality is a fundamental property of behavior, it is not currently understood how individual differences in brain structure and physiology produce idiosyncratic behaviors. Here we present evidence for idiosyncrasy in olfactory behavior and neural responses in *Drosophila*. We show that individual female *Drosophila* from a highly inbred laboratory strain exhibit idiosyncratic odor preferences that persist for days. We used in vivo calcium imaging of neural responses to compare projection neuron (second-order neurons that convey odor information from the sensory periphery to the central brain) responses to the same odors across animals. We found that, while odor responses appear grossly stereotyped, upon closer inspection, many individual differences are apparent across antennal lobe (AL) glomeruli (compact microcircuits corresponding to different odor channels). Moreover, we show that neuromodulation, environmental stress in the form of altered nutrition, and activity of certain AL local interneurons affect the magnitude of interfly behavioral variability. Taken together, this work demonstrates that individual *Drosophila* exhibit idiosyncratic olfactory preferences and idiosyncratic neural responses to odors, and that behavioral idiosyncrasies are subject to neuromodulation and regulation by neurons in the AL.

odor preference | individuality | sensory stimuli | neural encoding | neuromodulation

Olfaction is a deeply personal sense. We know from common experience that smells elicit strong experience-dependent and -independent reactions. Behavioral responses to an odor (e.g., durian or gasoline) can vary greatly among individuals, from attraction to utter aversion. The mechanisms by which volatile molecules are mapped into perceptual space (1, 2) and drive behavior are not well understood. In humans, both sociocultural experience (3) and genetic polymorphisms in odorant receptors (4) explain some individual variation in odor perception. Presumably, such sensory variation affects downstream neural responses, and thus odor perception, but currently little is known about how this idiosyncrasy manifests in the activity of neural circuits. A major obstacle to studying idiosyncrasy in odor circuits is the need to identify corresponding circuit elements across individuals. This is difficult in large organisms, where individual neurons are not identifiable or directly comparable across individuals. Moreover, establishing that specific circuit elements shape the distribution of behavioral responses across individuals requires large sample sizes (precisely measuring a distribution requires assessing rare individuals in its tails). This requirement essentially precludes the use of mammals for such studies.

We addressed these challenges by leveraging the identifiable and grossly stereotyped neuroanatomy of the antennal lobe (AL) of the fruit fly, *Drosophila melanogaster*. The *Drosophila* AL has around 50 identifiable odor-coding channels, which are arranged into spatially distinct glomeruli (5–7). The glomeruli are stereotyped with respect to their sensory neuron inputs, shape and size, and efferent innervation by projection neurons (PNs) that convey odor information deeper into the brain (8–10). Overlaid on

this coarse stereotypy, however, is a complex network of AL local neurons (LNs) providing dense interglomerular connections (11, 12). The roles of LNs in tuning AL odor responses are diverse (11–13) and may offer several mechanisms for diversifying individual odor responses in the AL. Notably, there are far more anatomical classes of LNs across individuals than there are LNs in an individual fly (11), implying that the complement of LNs in each fly is unique.

Individuality in *Drosophila* behavior has been observed in phototaxis (14), spontaneous locomotor biases (15), thermal preference (16), spontaneous microbehaviors (17), and object-fixated locomotion (18). These differences persist over days and represent something like fly personality. Individual behavior likely arises in part through stochastic events during development (19), and genetic factors determine the magnitude of behavioral variability in isogenic populations (20). Additionally, postdevelopmental activity of specific neural circuits also tunes individuality, meaning the nervous system can potentially control variability in real time (14, 15). It is likely that these factors are at work in regulating individual odor preferences, but the extent to which individual nervous systems represent the same stimulus differently has not been examined in this context. Using an automated odor-preference assay, we measured significant individuality in odor preference that was stable

Significance

Individuality is a fundamental feature of behavior. For instance, the same smell or song may evoke very different responses in 2 individuals. What is the biological basis for these differences? While behavioral differences likely originate with differences in neural activity, little is known about how idiosyncratic behavioral differences are reflected in neural activity. We used statistical behavioral analysis and live brain imaging to assess idiosyncratic odor responses in fruit flies, and found that the same odors produce different behavioral responses across flies and that these odors evoke subtly different patterns of brain activity across flies. Moreover, neuromodulators and sets of neurons in the olfactory region of the fly's brain directly modulate the degree of fly-to-fly behavioral variability in a flexible way.

Author contributions: K.S.H., M.A.-Y.S., G.C.T., and B.L.d.B. designed research; K.S.H., M.A.-Y.S., M.A.C., and B.L.d.B. performed research; K.S.H., M.A.-Y.S., and B.L.d.B. contributed new reagents/analytic tools; K.S.H., M.A.-Y.S., M.A.C., G.C.T., and B.L.d.B. analyzed data; and K.S.H., M.A.-Y.S., M.A.C., G.C.T., and B.L.d.B. wrote the paper.

Conflict of interest statement: B.L.d.B. is a scientific advisor for FlySorter, LLC. The authors have no additional conflicts.

This article is a PNAS Direct Submission. M.B.S. is a guest editor invited by the Editorial Board.

Published under the PNAS license.

Data deposition: All data and code needed to reproduce our findings and figures are available at <https://zenodo.org/record/3365688>. These files are also hosted, along with a readme, at <http://lab.debivort.org/odor-variability>.

¹K.S.H. and M.A.-Y.S. contributed equally to this work.

²To whom correspondence may be addressed. Email: debivort@oeb.harvard.edu.

This article contains supporting information online at www.pnas.org/lookup/suppl/doi:10.1073/pnas.1901623116/-DCSupplemental.

across days. Using volumetric 2-photon microscopy, we observed individuality in the representation of odors in the AL. Pharmacological and thermogenetic experiments established that multiple LN subsets and neuromodulatory axes appear to affect odor-preference individuality, forming a circuit with the potential to dynamically tune odor-preference variability in response to environmental cues.

Results

To determine whether individual flies exhibit idiosyncratic odor behaviors, we built an instrument to simultaneously measure the odor preference of 15 isolated flies (Fig. 1A), where each fly moves freely through a linear corridor in which 2 odor stimuli are pumped (21). The airflow bearing these odor cues is laminar, forming a sharp boundary between the 2 odor compartments at

the middle of the corridor. From there the airflow vents to the room (Fig. 1B and *SI Appendix*, Fig. S1A and B). Each experiment consisted of a 3-min “pre-odor period” in which filtered, dehumidified air was pumped into both compartments followed by a 3-min “odor-choice period” when alternative odor stimuli filled each half of each arena, lastly followed by a 30-s “post-odor period” of filtered, dehumidified air (Fig. 1C). In this setup, flies expressed olfactory preference by walking into and staying in their preferred odor compartment (Fig. 1C).

We observed a broad distribution of odor-preference scores in OCT–MCH (3-octanol vs. 4-methylcyclohexanol) choice experiments among highly inbred wild-type (*iso*^{KH11} strain; see *Methods*) females, reared in the same environment. Indeed, the observed distribution was broader than expected under a null model in which all animals sample their odor-choice behavior from the same distribution (Fig. 1D; $P < 0.001$), indicating that flies are behaving idiosyncratically. Additionally, the observed distribution of preference scores was broader than the distribution of “sham” scores calculated from the pre-odor period (gray lines in Fig. 1D and *SI Appendix*, Fig. S1C and D). Beyond the pair of aversive odorants OCT and MCH, we also observed idiosyncratic odor preferences (Fig. 1F) in experiments in which flies chose between filtered, dehumidified air and odorants 3-octanol, 1-butanol, and 2-heptanone. Importantly, we also confirmed that idiosyncratic preferences persist across days (Fig. 1E), as observed for other idiosyncratic fly behaviors (14–18). As a function of the interval between trials, the correlation (r) of fly odor preferences across trials was 0.23, 0.35, 0.35, and 0.24 respectively, for intervals of 0.16, 3, 24, and 96 h (Fig. 1E and *SI Appendix*, Fig. S1F–H).

Idiosyncratic behavior could have its basis in idiosyncratic patterns of odor-induced neural activity. We hypothesized that such response idiosyncrasies might be observable in the sensory periphery of the olfactory circuit, specifically in the glomeruli of the AL. To test this hypothesis, we delivered odorant stimuli to flies while imaging Ca^{2+} activity with a 2-photon microscope (Fig. 2A). We stimulated flies with 3 panels of odors (Fig. 2B). In the first 2 panels, 12 different odorants were delivered for 4 s each, with an ~80-s pause between odors, in a random order. In the third panel, OCT and MCH were delivered in alternation up to 5x each, with the same timing, starting randomly with OCT or MCH. We took 24-s volumetric recordings across AL glomeruli at ~0.8 Hz, acquiring GCaMP6m signal from dendrites of PNs (Fig. 2C) expressing GH146-Gal4.

As expected, we observed a variety of Ca^{2+} responses in PN dendrites (Fig. 2D and E and *SI Appendix*, Fig. S2), including excitatory and inhibitory responses to both odor onset and odor offset, depending on the glomerulus (Fig. 2D) and the odor (Fig. 2E). To characterize the population responses in PNs to each odor, we identified odor responses across many glomeruli using a semiautomated pipeline (*SI Appendix*, *Supplemental Methods*) that segmented glomeruli out of recording volumes (Fig. 2F1, G1, and H1). This let us characterize the odor responses of dozens of animals, to a dozen odors, in 3 to 15 glomeruli (mean = 10; *SI Appendix*, Fig. S2). We noticed that the responses of some glomeruli were very different across individuals, but consistent across multiple presentations of the odorant within an individual (Fig. 2F2, G2, and H2). To assess this systematically, we projected the multidimensional glomerulus-odor responses onto their first 2 principal components (Fig. 2I; see *SI Appendix*, Fig. S3 for eigenvalues and odor response covariance), where we observed that within-fly responses (i.e., across presentations) were, on average, closer than between-fly responses ($P = 0.012$ by bootstrap resampling). This was also true when we examined the responses of OCT and MCH specifically in the space of responses to the OCT/MCH stimulus panel (Fig. 2J and K; $P < 0.001$ and $P < 0.01$, respectively). This pattern was not an artifact of in-filling missing data for the principal component analysis (PCA), as it was also observed in smaller datasets with no missing data (*SI Appendix*, Fig. S4). Thus, neural responses to odors appear to differ significantly across individuals. Further

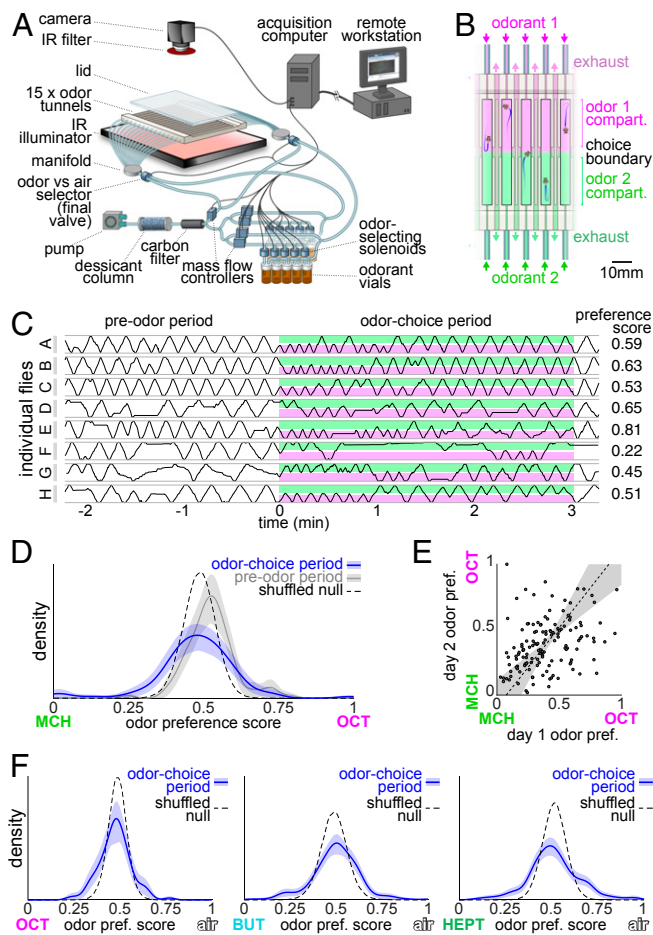


Fig. 1. Individual flies have idiosyncratic odor preferences. (A) Schematic of the odor-preference experimental apparatus. See *Methods*. (B) Schematic of the linear behavioral arenas, with an odorant flowing into each half. See *Methods* and *SI Appendix*, Fig. S1. The fraction of time a fly spends in a reference odor compartment is its preference score. (C) Kymographs showing the position in 8 individual flies over time. Color blocks indicate the 3-min odor-choice period when the 2 odors, OCT (magenta) and MCH (green), were delivered, with corresponding preference scores. (D) Distribution of OCT–MCH preference scores across isogenic wild-type animals. Kernel-density estimates during the odor-choice period (blue; shaded area is 95% CI) and pre-odor period (gray). Dotted line is the distribution under the null hypothesis that all flies have identical odor preferences. See *Methods*. Observed distribution is significantly broader than the null distribution ($P < 0.001$; by bootstrap resampling). (E) Scatterplot of individual OCT–MCH odor preferences on day 1 vs. day 2 ($r = 0.35$; $P < 0.0001$). Line is a linear fit. Shaded region is the 95% CI of the fit. (F) Distribution of OCT-, 1-butanol (BUT)-, and 2-heptanone (HEPT)-vs.-air preference scores. Plot elements as in D. Bootstrapped P values comparing null and observed distributions were all < 0.001 . See *Methods*.

analysis revealed that responses in specific glomeruli and to specific odors were varying idiosyncratic (SI Appendix, Fig. S5).

It was previously shown that the neuromodulator serotonin affects the degree of idiosyncrasy in phototaxis behavior (14). We tested whether neuromodulatory pathways also had an effect on odor-preference idiosyncrasy. We fed flies on food containing the serotonin synthesis inhibitor alpha-methyltryptophan (α -MW; 20 or 40 mM). These flies showed a dose-dependent reduction in variability compared to control flies. By contrast, feeding with the serotonin precursor 5-hydroxytryptophan (5-HTP) had little effect (Fig. 3A). Flies bearing a mutant allele of the *Dop1R1* dopamine receptor gene (*Dop1R1*¹⁰²⁶⁷⁶, hereafter “*Dop1R1*”) (22), exhibited lower variability than control flies (Fig. 3B). Conversely, flies fed the dopamine precursor L-DOPA (22) exhibited higher variability. The lower variability of *Dop1R1* is not explained by anosmia, as these flies exhibited reversal behaviors at the odor boundary during the odor-choice period (SI Appendix, Fig. S6 and Table S1).

We realized that our experimental manipulations changed not only the variability of behavior, but also its mean, and in our measurements, mean and variance are coupled. We also suspected that seasonal effects, such as those that affect olfactory conditioning (23), might also affect our behavior (indeed, variability was apparently higher in the winter, SI Appendix, Fig. S7 A–D). Additionally, we had more confidence in our estimate of some individuals’ preferences than others—flies that walk more perform more choices. We implemented a Bayesian linear model (Fig. 3C) to estimate and control for each of these effects, uncouple mean and variance, and assign more inference weight to flies that were more active. See Methods and SI Appendix, Table S2 and Fig. S7E. The output of this analysis was posterior distributions for the variance effects of genotype, experimental condition, and genotype-by-experimental condition parameters corresponding to our neuromodulatory manipulations (Fig. 3D). From these posteriors (Fig. 3D), more so than any individual experiment, we can infer that 5-HTP has no strong effect on variability, while α -MW had a substantial negative, dose-dependent effect, *Dop1R1* reduced variability substantially, and L-DOPA increased it.

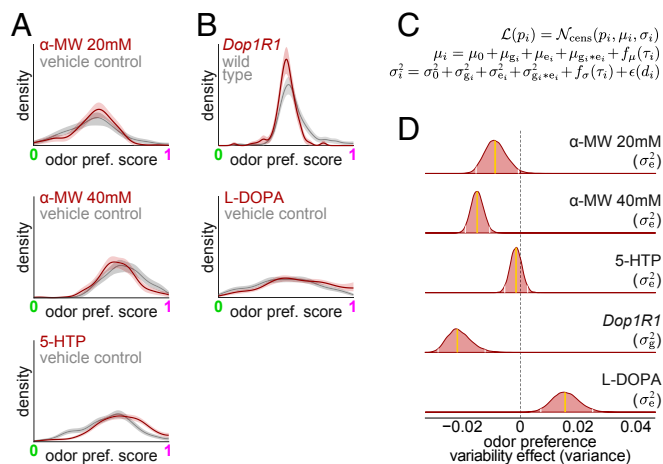


Fig. 3. Neuromodulation of behavioral individuality. (A) Sample single-experiment distributions of OCT–MCH preference scores across isogenic wild-type animals in control (gray) and drug (red) conditions. Lines are kernel density estimates; shaded areas are 95% CIs. Experiments: flies fed (for 3 d) 20 mM α -MW (Top), 40 mM α -MW (Middle), and 50 mM 5-HTP (Bottom). (B) As in A for manipulations of dopamine signaling. (Top) *Dop1R1*¹⁰²⁶⁷⁶ and a genetic control. (Bottom) Observed distributions for flies fed 5 mg/mL L-DOPA or vehicle for 3 d. (C) Model used to estimate the effects on odor-preference variability of neuromodulation manipulations. See Methods. (D) Posterior distributions of the model parameters for each manipulation. Gold lines indicate the mean of the posterior, white lines indicate edges of the 95% credible interval. Posterior distributions heavily overlapping 0 (dotted line) indicate no effect.

We also imaged PN Ca^{2+} responses in PN dendrites of flies that had been fed α -MW and controls (SI Appendix, Fig. S8). We again saw the signal of idiosyncratic neural coding (SI Appendix, Fig. S4B), but no significant difference between α -MW fed and controls (though there may have been some changes in the variability of coding in specific odors and glomeruli) (SI Appendix, Fig. S9 F and G). Using ELISAs, we confirmed that our drug treatments had the anticipated effects on the concentrations of serotonin and dopamine in fly heads (SI Appendix, Fig. S10).

Next, we sought to examine the neural circuit basis of the modulatory effects on behavioral variability. We used thermogenetic effectors to activate or inhibit circuit elements within the olfactory system and recorded the odor preferences of many individuals subject to this manipulation (Fig. 4 A–C). First we targeted the contralateral serotonin-immunoreactive deutocerebral (CSD) neurons (24) using 2 Gal4 lines. These serotonin-positive neurons have postsynaptic compartments distributed widely across the olfactory system and project axons into the AL contralateral to their cell body. Applying the Bayesian framework to infer the effects of these thermogenetic manipulations (Fig. 4D and SI Appendix, Fig. S11), we found no evidence that activating CSD neurons with dTRPA1 (an effector that depolarizes neurons at high temperatures; ref. 25) affected variability (Fig. 4E).

While CSD neurons apparently have no effect on variability, the AL local neurons express multiple serotonin receptors (26) and are potential regulators of variability as they have highly variable morphology across individuals (11). We found that activating or inhibiting different populations of LNs often had the effect of reducing behavioral variability. Specifically, the following genotypes were found to have variance-reducing effects at the induced temperature: *R14H04>dTRPA1*, *R14H04>Shibire^{ts}* (probably), *R46E11>dTRPA1*, *VT046560>dTRPA1*, and *VT046560>Shibire^{ts}*. (The *Shibire^{ts}* effector blocks vesicular release at the restrictive temperature) (27). These lines express Gal4 in different subsets of LNs of varying size and, presumably, varying physiology. Lastly, we manipulated the activity of tachykinin-expressing (Tk+) neurons (using R61H07-Gal4) (28), which overlap with a specific subset of LNs. We found that activating Tk+ cells with dTRPA1 probably increased variability, while silencing them had no effect. Thus, the effect of thermogenetically perturbing Tk+ cells appears to be inconsistent with the variability-reducing effect of perturbing LNs.

Neuromodulatory dynamics in the AL have been previously implicated in changing odor-induced responses in a satiety-dependent manner (29). We hypothesized that subjecting flies to dietary stress by switching between 2 kinds of food might increase behavioral variability, potentially as a bet-hedging response (i.e., when the environment fluctuates, diversify stimulus responses to increase the chance that some individuals are fit in the new environment) (16). We reared flies on cornmeal/dextrose food before switching them onto reconstituted flake food (Formula 4-24 [F4-24] from Carolina Biological Supply) for 1 d. (As controls, we switched them to fresh cornmeal/dextrose food and, alternatively, fed them flake food continuously.) This dietary switch caused higher variability (SI Appendix, Fig. S13). In contrast, flies chronically fed on F4-24 flake food showed lower variability than controls. Feeding the flies α -MW partially blocked the variability-increasing effects of the food shock, consistent with our earlier pharmacological experiments (Fig. 3 A and D).

Discussion

Odors evoke highly individualized perceptions. We set out to study this in a genetic model system with high-throughput behavioral assays and circuit-mapping tools. We observed that flies have persistent idiosyncratic preferences when choosing between 2 olfactory stimuli (Fig. 1). A challenge in our analyses was the limited window in which flies expressed an odor preference (roughly 3 min) before appearing to habituate (30) (Fig. 1C), which likely underlies the modest day-to-day repeatability of individual odor preferences ($r = 0.35$; Fig. 1E) compared to other measures of fly personality (14–16, 18). This partly motivated

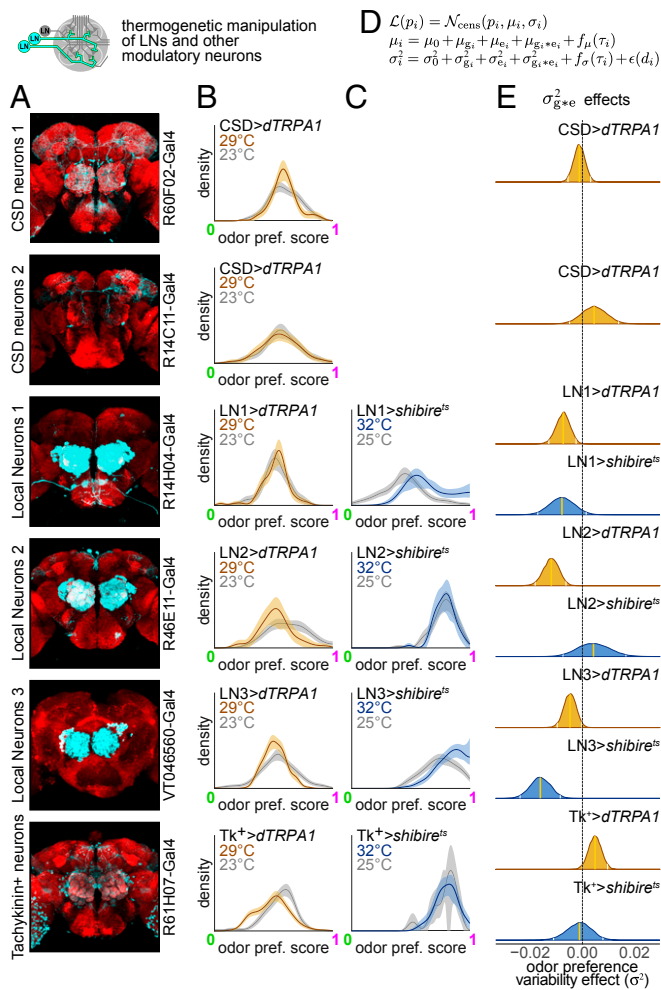


Fig. 4. Local neurons in the antennal lobe modulate individuality of odor preference. **(A)** Confocal micrographs of expression patterns targeting serotonin-immunoreactive CSD neurons, local neurons, and tachykinin-positive neurons. Red background stain is anti-nc82 staining synaptic active zones. (The red channel of the VT046560 image is also stained for anti-DLG.) Cyan is mCD8-GFP driven by each Gal4 line. Images of all *Janelia FlyLight* Gal4 lines reproduced and modified with permission from the *Janelia FlyLight* team. **(B)** Sample single-experiment kernel density estimates of the distribution of OCT-MCH preference scores for flies expressing the thermogenetic activator *dTRPA1* driven by each Gal4 line. Gray distributions are at the permissive temperature (23 °C), gold distributions, the restrictive temperature (29 °C). **(C)** As in **B**, but for animals expressing *Shibire^{TS}* at permissive (25 °C) and restrictive (32 °C) temperatures. **(D)** Model used to estimate the effects on odor-preference variability of these neural circuit manipulations. Experimental condition terms (*e*) denotes the temperature of the experiment, and genotype terms (*g*), index animals of the background genotype (*iso^{KH11}*), parental genotype controls (*Gal4/+*, *UAS-shibire^{TS}/+*, and *UAS-dTRPA1/+*), and experimental *F₁s* (*Gal4/UAS-shibire^{TS}* and *Gal4/dTRPA1*). The *g * e* term accounts for the thermogenetic interaction of *F₁* genotypes and temperature. **(E)** Posterior distributions of the effect on odor-preference variability of silencing (blue) or activating (gold) neurons of each Gal4 line using *shibire^{TS}* or *dTRPA1*, respectively. Gold lines indicate the mean of the posterior, and white lines, the edges of the 95% credible interval. Posterior distributions heavily overlapping 0 (dotted line) indicate no effect.

our use of Bayesian modeling to assess the effects of our manipulations.

Despite the anatomical and functional stereotypy of the peripheral olfactory system, we observed individuality in odor coding across glomeruli of the AL (Fig. 2). Some of this individuality may be due to artifacts of dissection, mounting, or variable expression

of the Ca^{2+} indicator. Still, the observation of glomerular responses to an odorant that are consistently excitatory in one fly, but consistently inhibitory in another, is not easily attributable to such artifacts. We imaged PN responses, which are more broadly tuned than olfactory receptor neuron (ORN) representations (31), and the circuit dynamics that underlie this broadening may also contribute to distinguishing representations across individuals. The significance of our observed Ca^{2+} response differences may ultimately come down to predicting idiosyncratic behaviors from idiosyncratic coding, as a circuit may produce consistent outputs even with idiosyncratic internal states (32). For now, we believe that the prevailing view that odor responses in the AL are highly stereotyped across individuals should be tempered.

Neuromodulatory axes regulate the amount of behavioral variability in isogenic animals; disrupting serotonin increased variability in fly phototaxis (14), while in *Caenorhabditis elegans*, it decreased variability in locomotor activity (33). Indeed, we observed that *Dop1R1* mutation strongly decreased odor-preference variability (conversely, feeding flies L-DOPA increased variability; Fig. 3). Inhibiting serotonin had a dose-dependent effect of decreasing variability in odor preference. The Bayesian framework we used to infer these effects also revealed a striking environmental effect. Odor-preference variability was consistently higher in the winter (*SI Appendix, Fig. S7*). This effect was large, despite our rearing flies in temperature- and humidity-controlled incubators and measuring behavior in temperature- and humidity-controlled environmental rooms. We suspect that outdoor air temperature is only a correlate of the true seasonal cause of fluctuating variability, for which there are many possibilities, including plant or yeast volatiles or barometric pressure.

Acutely activating the serotonin-immunopositive CSD neurons had no effect on behavioral variability (Fig. 4E), in contrast with serotonin pharmacological experiments, but consistent with a reported lack of effect on AL activity (34). The long timescale of serotonin effects on behavioral variability may reflect a role in regulating neurite structure, consistent with its role in neurodevelopment (35). Many cell types in the AL express a diversity of serotonin receptors (26) and may mediate the effect of serotonin manipulation on behavioral variability. These include the LNs, which, when silenced or activated, resulted in lower odor-preference variability (Fig. 4; and, presumably, a less sparse and regularized pattern of PN activity) (36). This suggests an endogenous role of increasing variability, consistent with their morphological variability across individuals (11). Three experimental manipulations reduced variability: thermogenetic perturbation of LNs, serotonin synthesis inhibition, and mutation of *Dop1R1*, which suggest that the endogenous role of these factors is to increase odor-preference variability across individuals. *Dop1R1* facilitates synaptic plasticity in the mushroom body (MB) in support of associative conditioning (22, 37), but we found that thermogenetic manipulations of the MB had no effect on variability (*SI Appendix, Fig. S11*). Perhaps the effect of dopamine is in the central complex, where it is known to modulate locomotion (38). Indeed, the reversal behavior seen at the odor boundary may be supported by idiothetic path integration implemented in the central complex (39, 40).

Endogenous biological mechanisms that increase variability could underlie bet-hedging strategies (16, 19) under the control of the nervous system. Such strategies could respond rapidly to environmental fluctuations to diversify behavior and allow individuals to exhibit behavioral phenotypes fit for the new environment. We tested this notion by subjecting flies to a rapid change in their food, from their normal cornmeal/dextrose food to a commercial flake food on which flies grow less successfully (41). This acute food shock caused an increase in odor-preference variability (*SI Appendix, Fig. S13*). Feeding flies serotonin synthesis inhibitor during this food shock diminished the increase in variability. Taken together, these findings suggest that odor-preference variability is under the acute control of several specific neuron types in the AL and possibly elsewhere,

and over longer timescales by neuromodulation. These axes of flexibility may facilitate bet-hedging strategies by which animals can respond to environmental fluctuations with adaptive changes in behavioral diversity.

Methods

See *SI Appendix, Supplementary Methods* for details.

Data and Code Repositories. All data and code needed to reproduce our findings and figures are available in ref. 42. These files are also hosted, along with a readme at <http://lab.debivort.org/odor-variability>. Raw imaging files are available on request.

Fly Care and Behavior. All transgenic lines were outcrossed to a common isogenic background (iso^{KH11}) for 10 generations. Flies were grown on cornmeal/dextrose food in incubators (25 °C, 40% relative humidity, 12:12 h light:dark cycle), and behavior experiments were conducted on females 3 to 4 d posteclosion. Flies were aspirated directly into behavioral arenas without anesthetization. Odors were delivered to each of the behavioral arenas using an array of odorant vials; the flow through vials was set by computer-controlled solenoids and mass-flow controllers. Individual preference was measured as the fraction of time each individual spent in the half of the arena with a reference odor. Between day-to-day persistence experiments, flies were housed singly in fly plates (FlySorter, LLC).

Imaging and Analysis. Flies for Ca²⁺ imaging were mounted beneath a foil sheet in a custom 2-photon stage. Under saline, a needle was used to remove the cuticle over the ALs. Odors were delivered to the antennae in a manner similar to the behavioral experiment (Fig. 2A). GCaMP6m responses in PNs (driven by GH146-Gal4) were acquired from a volume that included all glomeruli at a rate of 0.833 Hz for 24 s for each odor. For most analyses, the

response of a glomerulus to a particular odorant was taken as the integrated $\Delta F/F$ for seconds 7 through 13 of the recording (Fig. 2 B, D, and E).

Behavior Modeling. To estimate the effects of environment (pharmacological and nutrient experiments), genotype (Dop1R1 vs. wild type) and genotype by environment (thermogenetic circuit manipulations) on behavioral variability, we implemented 3 Bayesian linear models of mean and variance effects (Figs. 3C, 4D, and *SI Appendix, Fig. S13B*). These models accounted for 1) odor-preference scores being censored by their [0,1] domain, 2) odor variability changing seasonally (*SI Appendix, Fig. S7A*), and 3) the odor preference of flies that were less active during the odor-choice period being harder to estimate. These models were fit in the Stan framework in R (43) to estimate posterior distributions on each effect, using weakly informative priors estimated with preliminary experiments.

Pharmacology. Flies fed manipulators of serotonin and dopamine signaling were placed on cornmeal/dextrose media or F4-24 flake food that was made fresh for each experiment by melting the media and mixing it with stock drug, or by reconstituting flake food in drug-containing water. Neuromodulator in vivo concentration was assessed by ELISAs.

ACKNOWLEDGMENTS. We thank Katrin Vogt and Carolyn Elya for helpful comments on the manuscript, Ed Soucy and Joel Greenwood of Harvard's Center for Brain Science Neuroengineering core for their help building the 2-photon microscope, the Research Computing Group at Harvard University for operating the Odyssey cluster used for model fitting, and Jess Kanwal and Kyobi Skutt-Kakaria for insightful discussions. B.L.d.B. was supported by a Sloan Research Fellowship, a Klingenstein-Simons Fellowship Award, a Smith Family Odyssey Award, a Harvard/MIT Basic Neuroscience Grant, and National Science Foundation grant no. IOS-1557913. G.C.T. was supported by the Howard Hughes Medical Institute. M.A.-Y.S. was supported by Harvard's Quantitative Biology Initiative.

1. A. Keller *et al.*, DREAM Olfaction Prediction Consortium, Predicting human olfactory perception from chemical features of odor molecules. *Science* **355**, 820–826 (2017).
2. A. A. Koulovskov, B. E. Kolterman, A. G. Enikolopov, D. Rinberg, In search of the structure of human olfactory space. *Front. Syst. Neurosci.* **5**, 65 (2011).
3. A. Keller, M. Hempstead, I. A. Gomez, A. N. Gilbert, L. B. Vosshall, An olfactory demography of a diverse metropolitan population. *BMC Neurosci.* **13**, 122 (2012).
4. J. D. Mainland *et al.*, The missense of smell: Functional variability in the human odorant receptor repertoire. *Nat. Neurosci.* **17**, 114–120 (2014).
5. A. Couto, M. Alenius, B. J. Dickson, Molecular, anatomical, and functional organization of the Drosophila olfactory system. *Curr. Biol.* **15**, 1535–1547 (2005).
6. E. Fishilevich, L. B. Vosshall, Genetic and functional subdivision of the Drosophila antennal lobe. *Curr. Biol.* **15**, 1548–1553 (2005).
7. P. P. Laisue, L. B. Vosshall, The olfactory sensory map in Drosophila. *Adv. Exp. Med. Biol.* **628**, 102–114 (2008).
8. H.-H. Lin, J. S.-Y. Lai, A.-L. Chin, Y.-C. Chen, A.-S. Chiang, A map of olfactory representation in the Drosophila mushroom body. *Cell* **128**, 1205–1217 (2007).
9. G. S. X. E. Jefferis *et al.*, Comprehensive maps of Drosophila higher olfactory centers: Spatially segregated fruit and pheromone representation. *Cell* **128**, 1187–1203 (2007).
10. M. Figeš, R. I. Wilson, Stereotyped connectivity and computations in higher-order olfactory neurons. *Nat. Neurosci.* **17**, 280–288 (2014).
11. Y.-H. Chou *et al.*, Diversity and wiring variability of olfactory local interneurons in the Drosophila antennal lobe. *Nat. Neurosci.* **13**, 439–449 (2010).
12. Y. Seki, J. Rybak, D. Wicher, S. Sachse, B. S. Hansson, Physiological and morphological characterization of local interneurons in the Drosophila antennal lobe. *J. Neurophysiol.* **104**, 1007–1019 (2010).
13. S. M. Kim, C.-Y. Su, J. W. Wang, Neuromodulation of innate behaviors in Drosophila. *Annu. Rev. Neurosci.* **40**, 327–348 (2017).
14. J. S. Kain, C. Stokes, B. L. de Bivort, Phototactic personality in fruit flies and its suppression by serotonin and white. *Proc. Natl. Acad. Sci. U.S.A.* **109**, 19834–19839 (2012).
15. S. M. Buchanan, J. S. Kain, B. L. de Bivort, Neuronal control of locomotor handedness in Drosophila. *Proc. Natl. Acad. Sci. U.S.A.* **112**, 6700–6705 (2015).
16. J. S. Kain *et al.*, Variability in thermal and phototactic preferences in Drosophila may reflect an adaptive bet-hedging strategy. *Evolution* **69**, 3171–3185 (2015).
17. J. G. Todd, J. S. Kain, B. L. de Bivort, Systematic exploration of unsupervised methods for mapping behavior. *Phys. Biol.* **14**, 015002 (2017).
18. G. Linneweber, M. Andriatsilavo, S. Dutta, L. Hellbruegge, A neurodevelopmental origin of behavioral individuality. *bioRxiv:10.1101/540880* (5, February 2019).
19. K. Honnegger, B. de Bivort, Stochasticity, individuality and behavior. *Curr. Biol.* **28**, R8–R12 (2018).
20. J. F. Ayroles *et al.*, Behavioral idiosyncrasy reveals genetic control of phenotypic variability. *Proc. Natl. Acad. Sci. U.S.A.* **112**, 6706–6711 (2015).
21. A. Claridge-Chang *et al.*, Writing memories with light-addressable reinforcement circuitry. *Cell* **139**, 405–415 (2009).
22. Y.-C. Kim, H.-G. Lee, K.-A. Han, D1 dopamine receptor dDA1 is required in the mushroom body neurons for aversive and appetitive learning in Drosophila. *J. Neurosci.* **27**, 7640–7647 (2007).
23. P. Szyszka *et al.*, Mind the gap: Olfactory trace conditioning in honeybees. *J. Neurosci.* **31**, 7229–7239 (2011).
24. B. Roy *et al.*, Metamorphosis of an identified serotonergic neuron in the Drosophila olfactory system. *Neural Dev.* **2**, 20 (2007).
25. F. N. Hamada *et al.*, An internal thermal sensor controlling temperature preference in Drosophila. *Nature* **454**, 217–220 (2008).
26. T. R. Sizemore, A. M. Dacks, Serotonergic modulation differentially targets distinct network elements within the antennal lobe of Drosophila melanogaster. *Sci. Rep.* **6**, 37119 (2016).
27. T. Kitamoto, Conditional modification of behavior in Drosophila by targeted expression of a temperature-sensitive shibire allele in defined neurons. *J. Neurobiol.* **47**, 81–92 (2001).
28. K. Asahina *et al.*, Tachykinin-expressing neurons control male-specific aggressive arousal in Drosophila. *Cell* **156**, 221–235 (2014).
29. K. I. Ko *et al.*, Starvation promotes concerted modulation of appetitive olfactory behavior via parallel neuromodulatory circuits. *eLife* **4**, e08298 (2015).
30. S. Das *et al.*, Plasticity of local GABAergic interneurons drives olfactory habituation. *Proc. Natl. Acad. Sci. U.S.A.* **108**, E646–E654 (2011).
31. V. Bhandawat, S. R. Olsen, N. W. Gouwens, M. L. Schlieff, R. I. Wilson, Sensory processing in the Drosophila antennal lobe increases reliability and separability of ensemble odor representations. *Nat. Neurosci.* **10**, 1474–1482 (2007).
32. D. J. Schulz, J.-M. Goillard, E. Marder, Variable channel expression in identified single and electrically coupled neurons in different animals. *Nat. Neurosci.* **9**, 356–362 (2006).
33. S. Stern, C. Kirst, C. I. Bargmann, Neuromodulatory control of long-term behavioral patterns and individuality across development. *Cell* **171**, 1649–1662 (2017).
34. X. Zhang, Q. Gaudry, Functional integration of a serotonergic neuron in the Drosophila antennal lobe. *eLife* **5**, e16836 (2016).
35. P. A. Sykes, B. G. Condron, Development and sensitivity to serotonin of Drosophila serotonergic varicosities in the central nervous system. *Dev. Biol.* **286**, 207–216 (2005).
36. S. R. Olsen, V. Bhandawat, R. I. Wilson, Divisive normalization in olfactory population codes. *Neuron* **66**, 287–299 (2010).
37. H. Qin *et al.*, Gamma neurons mediate dopaminergic input during aversive olfactory memory formation in Drosophila. *Curr. Biol.* **22**, 608–614 (2012).
38. B. Kottler, R. Faville, J. C. Bridi, F. Hirth, Inverse control of turning behavior by dopamine D1 receptor signaling in columnar and ring neurons of the central complex in Drosophila. *Curr. Biol.* **29**, 567–577 (2019).
39. R. A. Corfas, M. H. Dickinson, Diverse food-sensing neurons trigger idiothetic local search in Drosophila. *bioRxiv:10.1101/433771* (3 October 2018).
40. K. S. Kakaria, B. L. de Bivort, Ring attractor dynamics emerge from a spiking model of the entire protocerebral bridge. *Front. Behav. Neurosci.* **11**, 8 (2017).
41. K. G. Ormerod *et al.*, Drosophila development, physiology, behavior, and lifespan are influenced by altered dietary composition. *Fly (Austin)* **11**, 153–170 (2017).
42. K. S. Honnegger, M. A.-Y. Smith, M. A. Churgin, G. C. Turner, B. L. de Bivort, Idiosyncratic neural coding and neuromodulation of olfactory individuality in Drosophila. Zenodo. <https://zenodo.org/record/3365688>. Deposited 14 August 2019.
43. Stan Development Team, Stan User's Guide Version 2.18. <https://mc-stan.org/docs/2.18/stan-users-guide/index.html>. Accessed 11 August 2019.

Supplementary materials for: Idiosyncratic neural coding and neuromodulation of olfactory individuality in *Drosophila*

Kyle Honegger^{1,2,†}, Matthew Smith^{1,†}, Matthew Churgin¹, Glenn Turner³, Benjamin de Bivort^{1*}

1 — Department of Organismic and Evolutionary Biology & Center for Brain Science, Harvard University, Cambridge, MA 02138

2 — Ann & Robert H. Lurie Children's Hospital of Chicago, Chicago, IL 60611

3 — Janelia Research Campus, Howard Hughes Medical Institute, Ashburn, VA 20147

† — contributed equally

* — correspondence: debivort@oeb.harvard.edu

Supplementary Methods

Data and code repositories

All data needed to reproduce our findings and figures, along with all analysis code is available for download at <http://zenodo.org/record/3365688>. These files are also hosted, along with a readme companion page at <http://lab.debivort.org/odor-variability>. Raw imaging files are available on request to the corresponding author.

Fly stocks

The following stocks were obtained from the Bloomington *Drosophila* Stock Center: P{GMR14C11-GAL4}attP2 (BDSC #49256), P{GMR60F02-GAL4}attP2 (#48228), P{GMR61H07-GAL4}attP2 (#39282), P{GMR14H04-GAL4}attP2 (#48665), P{GMR46E11-GAL4}attP2 (#50272), UAS-dTrpA1 (#26263), and P{20XUAS-IVS-GCaMP6m}attP40 (#42748). The VT046650-GAL4 (VDRC ID #204702) driver was obtained from Vienna *Drosophila* Resource Center, and the GH146-GAL4 and *Dop1R1* lines were generously provided by Y. Zhong and J. Dubnau,

respectively. The PBac{20XUAS-TTS—shi[ts1]-p10}attP2 line and the split-GAL4 line “MB010B” (13F02-p65ADZp/CyO; 52H09-ZpGdbd) were generously provided by G. Rubin and Y. Aso.

Isogenic line iso^{KH11}

Our main control strain, the isogenic *Drosophila* line iso^{KH11}, was created by inbreeding the balancer-isogenized *w(isoCJ1)* strain of *w¹¹¹⁸* ([1]; shared by J. Dubnau) for 10 generations with full-sibling crosses. To equilibrate genetic background, all mutant and transgenic lines listed above were outcrossed to the iso^{KH11} line for at least 10 generations before being used in any imaging or odor preference experiments.

Fly rearing

Unless otherwise indicated, experimental flies were reared in a *Drosophila* incubator (Percival Scientific DR-36VL) under controlled conditions (25°C, 40% RH, 12:12h light:dark cycle) and fed a standardized cornmeal/dextrose medium [2] supplemented with activated yeast. Flies used for behavior were cultured under low-density conditions by allowing ~10 mated females 48-72 hours to lay eggs in a 500ml culture bottle containing folded Kimwipes and ~200ml medium.

Behavioral apparatus

The custom designed behavioral apparatus was constructed of Accura 60 plastic using stereolithography (In'Tech Industries) fabrication. Stainless steel hypo tubing (Small Parts) was used to connect the apparatus with Teflon odor tubes (ID: 0.7mm). The apparatus consisted of 15 parallel tunnels (50mm long, 5mm wide, 1.3mm tall), separated by 5mm spacers. Odorized or clean air was delivered through inlet ports at each end of the tunnel and streams vented to the room through exhaust ports in the center choice zone. An active vacuum was not applied to the exhaust ports, and the tunnels operated close to atmospheric pressure throughout the experiment. Clear acrylic was used as a base and lid for the apparatus. The lid was clamped in place above the apparatus to ensure an air-tight seal during odor presentation. Odors were presented using proportional air blending to control odor concentration. Air dilutions could be made independently for each side of the apparatus. A custom 15-way PEEK manifold was used on each side to split the odorized flow equally between 15 tunnel inlets. A final valve (SH360T041; NResearch) was used immediately upstream of each manifold to quickly switch between pure dehumidified air and the odorized stream. Based on simulation results (details below), airflow through the tunnels is expected to be laminar, and to form a sharp boundary between the two odor compartments at the middle of the corridor.

To maintain a consistent molar flux of odorant at different experimental temperatures, we used digital mass flow controllers to deliver 0.1SLPM air to the end of each tunnel. Because the density of a gas is a function of temperature, the volumetric flow of air increases with temperature to maintain a constant mass flow. Therefore, the velocity of air flowing through the tunnels increases with temperature, but the molar flux of odorant over the fly stays constant (ignoring changes in vapor pressure). The laminar air velocity in the direction of the center port was approximately 2.6cm/sec at 25°C, well within the range of wind speeds experienced by insects in a natural environment [3].

A three-dimensional Computational Fluid Dynamics (CFD) analysis was performed using Autodesk CFD (Autodesk, Inc., San Rafael, CA) software to model the flow of gas through the tunnels. CFD analysis revealed that flow through most of the length of each tunnel is laminar, with some turbulent flow in the center and near the inlet ports on each end (Figure S1A). A scalar mixing simulation, using a simulated tracer gas, revealed a steep mixing gradient for odor concentration, limited almost entirely to the center choice zone where the opposing odor streams meet (Figure S1B). These results are in general agreement with the behavior we observe.

Odor delivery

For imaging experiments, odors were delivered using a 12-channel serial-air-dilution olfactometer described in [4]. For behavioral experiments, odors were presented using a dual-path odor delivery system integrated into the behavioral apparatus. In both devices, desiccated air was filtered through an activated carbon trap (Agilent HT-200) before passing through digital mass flow controllers (MFCs; Alicat Scientific). For each odorant, 5ml of pure odorant was placed with a folded strip of filter paper in a 40ml glass vial fitted with a custom PTFE cap with inert fittings. The saturated headspace from these vials was combined with a variable carrier stream to produce between 10% and 20% saturated vapor, the range in which we observe a linear input-output relationship. All tubing was pure PTFE or PTFE coated for inertness. A photoionization detector (200B miniPID, Aurora Scientific) was used to periodically monitor the concentrations of test odors being delivered. The following odorants were obtained from Sigma-Aldrich: 2-heptanone (CAS#: 110-43-0), 1-pentanol (71-41-0), 3-octanol (589-98-0), hexyl-acetate (142-92-7), 4-methylcyclohexanol (589-91-3), pentyl-acetate (628-63-7), 1-butanol (71-36-3), ethyl-lactate (97-64-3), geranyl acetate (105-87-3), and 1-hexanol (111-27-34). Citronella and peppermint essential oils were purchased from Aura Cacia (items #191112 and #188840), and 200 proof ethanol from Decon Labs (V1001).

Behavior imaging

Flies were illuminated from beneath using a modified 15-inch laptop display panel (LP150X2; LG Philips) equipped with a high-density infrared LED array (peak emission 880nm). This approach produces homogeneous backlighting for high-contrast silhouette detection at a wavelength not visible to the fly. The screen was placed approximately 4cm below the behavioral apparatus to avoid heating the flies. We used a high-resolution CMOS camera (Point Grey Firefly MV USB) equipped with a zoom lens and longpass filter (Kodak Wratten Filter #87C) to collect images at 60Hz.

Behavior-tracking software

Custom MATLAB (The MathWorks, Inc.) routines were used to record and analyze the behavior of flies and control odor delivery. Tunnels and flies were automatically detected using 2D cross-correlation to align tunnel and fly outlines to template images. During an odor experiment, each frame was background subtracted to yield the silhouettes of the flies being assayed. For each time point, the centroid position, orientation, and major axis length of each silhouette were calculated and stored for offline analysis.

Behavioral experiments

Flies to be assayed for behavior were collected within 24 hours of eclosing and placed into a fresh vial containing fresh cornmeal/dextrose medium. Strictly, only females were used for behavior and imaging experiments. Vials each contained approximately 30 female flies, and were kept in the temperature and humidity-controlled incubator for 3 days, so that all flies were 3-4 days post-exclusion when tested. Flies were individually aspirated into the behavioral apparatus through a small hole in the lid. No anesthesia was used at any point on flies used in behavioral experiments. To minimize external causes of behavioral variability, odor preference assays were performed in an isolated temperature-controlled environmental chamber in total darkness. Behavioral assays began immediately after all flies were loaded and the lights were turned off. Each odor preference experiment ran for a total of 6 minutes and 30 seconds: 3 minutes of clean air, 3 minutes of air mixed with odorant, and 30 seconds of clean air post-odorant. The apparatus was partially disassembled and wiped down with absolute ethanol between experiments to remove any fly-deposited contamination. Prior to running behavioral experiments we adjusted odor concentrations so that the mean odor preference for OCT would be near 0.4. This was done by measuring the mean odor preference of a small number of *iso^{KH11}* flies prior to the behavior experiment, then adjusting concentrations via flow controllers and remeasuring mean preference.

Preference persistence experiments

Several experiments required storing and maintaining identities of individual flies across multiple days. For this we used FlyPlates (FlySorter LLC, Seattle, WA), which are modified 96-well plates with a mesh top and bottom. The plates were placed on a bed of cornmeal/dextrose fly medium and individual flies were aspirated into and out of each well, allowing identities to be maintained across multiple days. The food was replaced daily. To remove any potential contribution of between-tunnel differences in stimulus delivery to the across-day correlation, the tunnel assignment for each fly was randomly chosen each day.

Gal4 expression pattern images

Panels modified with permission from FlyLight images (Figure 4A) were downloaded from <http://flweb.janelia.org/cgi-bin/flew.cgi>. Confocal micrographs of expression patterns targeting, the red is the background stain for anti-nc82, and cyan is mCD8-GFP. The red channel of the VT046560 image is also stained for anti-DLG [5].) Cyan is mCD8-GFP [6] driven by the Gal4 line denoted.

Calcium imaging fly prep

Flies were collected from population bottles within 24 hours of eclosion. Those flies were put into vials with standard cornmeal/dextrose fly food for approximately 72 hours. Prior to mounting, single flies were cold anesthetized by being sealed in a plastic tube and submerged in ice. The anesthetized fly was then placed into a custom platform that exposed the fly head for removal of the cuticle and calcium imaging of the antennal lobe while keeping the antennae dry and exposed beneath the platform. The platform was a 3D printed 80mm diameter circle with a 5mm by 5mm square recessed into the center. At the bottom of the recess was a thin aluminum sheet (0.5mm) with a laser cut hole which allowed for the fly's head and thorax to be wedged between to stabilize the fly without damage. The fly's head was fixed to the stage by applying a small amount of UV (Loctite AA 3972) curing glue around the edge of both eyes to secure it the stage. The proboscis was then carefully extended and waxed to the bottom of the stage to further prevent movement of the head. We used a saline solution, as described in the methods of [7], to cover the exposed fly head and thorax and filling the small recessed section of the mounting stage. We used a sharpened 32-gauge needle to cut the cuticle of the fly and expose the antennal lobe.

Calcium imaging

GCaMP6m-expressing flies were imaged using a custom-built galvanometer-scanning two-photon microscope and ultrafast Ti:sapphire laser (Spectra-Physics Mai Tai) tuned to 930 nm. The microscope was controlled with a customized build of ScanImage 3.8 software (Vidrio Technologies, [8]). Custom MATLAB scripts were used to control stimulus delivery during imaging. Fast volume-scanning was

performed using a piezoelectric objective scanner (Physik Instrumente PIFOC PD72Z4), capable of continuous sawtooth movement in the Z dimension. Each volume was imported as a tiff stack and smoothed with a 3-dimensional gaussian kernel with standard deviation of 3 in all dimensions. A background was selected for every odor presentation per fly by pooling all volumes and taking pixels with intensity below the 25th percentile. At each time point, the mean of the background was calculated to generate a value for background subtraction. The resultant volumes were linearized into 1xn vectors and concatenated across time to create a matrix for *k*-means clustering (n-voxels by *k*-time points). Each voxel was z-scored across time, and *k*-means clustering was run using MATLAB R2018a's default KMEANS function with *k* = 36 and replicates = 15. For each cluster output by *k*-means, we applied a lenient size criterion that included only clusters composed of between 300 and 30,000 voxels. We then manually sorted through the remaining clusters to pick those that look reasonable in terms of geometry, size, and location, using a 3-dimensional *in-vivo Drosophila* antennal lobe atlas as a guide [9]. The selected clusters represented the glomeruli for each fly. This glomerulus mask was applied to the fly's odor block to yield $\Delta F/F$ traces for each glomerulus-odor pair within the fly. Within a single fly, separate *k*-means glomeruli masks were generated and applied for each odor presentation panel (12-odor panel-1, 12-odor panel-2, and the panel of OCT/MCH presentations). The matrix for principal component analysis was created by taking the integrated sum of $\Delta F/F$ for seconds 7-13 for each glomerulus-odor pair in an odor panel presentation, and z-scoring across flies. Whenever a glomerulus cannot be identified within a fly, the associated glomerulus-odor values for that fly are considered missing data. For our PCA matrix, we replaced any missing data within a fly with the mean across all flies of that specific odor-glomerulus value.

Thermogenetics

The thermogenetic effectors, UAS-shibire^{ts} and UAS-dTrpA1, were obtained from Bloomington Stock Center and backcrossed for at least ten generations into our isogenic line *iso*^{KH11}. For behavioral experiments, each effector was crossed to a GAL4 driver line and F₁s were used for the experiment. TrpA1 F₁s were tested at 23°C (permissive temperature control condition) or 29°C (restrictive; TRPA1 active). Shibire^{ts} F₁s were tested at 25°C (permissive temperature control condition) or at 32°C (restrictive; Shibire^{ts} blocking vesicle release). Animals in the restrictive condition were incubated for 30 minutes at 32°C prior to testing.

Pharmacology

Flies used for drug treatment experiments were placed on food that was supplemented with either α -MW, 5-htp, or L-DOPA. To create the drug food mixture, the drug was mixed into water solution and diluted to the appropriate concentration with melted cornmeal/dextrose standard medium or F4-24 flake

food, then placed into an empty plastic vial (Genesee scientific 32-116). The flies were flipped onto freshly made drug-supplemented food daily for the 72 hours post eclosion.

Food-induced environmental stress

Formula 4-24 (F4-24) prepared food mix was purchased from Carolina Biological Supply Company (item #173120). Portions of this dry media mix were processed in a coffee grinder to achieve a uniform density and mixed with tap water with a ratio of 1:1. For the food shock experiments we placed newly eclosed flies onto cornmeal/dextrose medium for 48 hours, then switched to F4-24 food for the remaining 24 hours prior to evaluating behavior.

Behavioral analysis

All behavioral analyses were performed using R-3.5.1 [8] or MATLAB R2018b. Behavioral analyses consisted of both model-based (estimating effects of experimental manipulations) and non model-based (individuality scores and distribution visualizations) inference. For non model-based analyses we included only flies that met a minimum activity threshold of 25 cm of distance traveled during the odor period, since highly inactive flies can substantially skew the analysis. For model-based analyses we adjust for group differences in activity level, so we included all flies that entered the choice zone of the tunnel at least once during the experiment.

Individuality scores were calculated as $\text{Var}_{\text{obs}} - \text{Var}_{\text{null}}$. Though MAD as a measure of dispersion is preferable to variance, as discussed below, we used variance to estimate individuality because its additive property makes the numerical difference between observed and null a meaningful quantity. The individuality score is interpretable as the amount of additional variance, supplied by stable inter-fly preference differences, beyond that expected from sampling error alone.

The expected “null model” variance was estimated from a distribution derived by Monte Carlo simulation. Briefly, we calculated a transition matrix representing the proportion of times flies crossed from one odor into the other, or entered the choice zone and then returned to the side they came from. Then we segmented tunnel position traces into a series of bout times - the time between entering an odorized portion of the tunnel and leaving it, and pooled them together according to odor. For a given group of flies, the collection of odor bouts preserves the overall mean preference, but discards the correlation of bouts observed within a fly. A population of virtual “Markov flies” equal to the number of observed flies was generated and each virtual fly was assigned an initial “odor choice.” For each virtual fly, a Markov chain of choices was generated from the empirical transition matrix, and each virtual choice was paired with an occupancy time sampled from the pool of bout times for its respective odor.

Samples were repeatedly taken from the chain until 3 minutes of simulated behavior was collected for each fly. From each Markov fly's simulated time series, we calculated the proportion of time spent in the reference odor and collected these preference scores across the virtual population. This procedure was repeated 1,000 times and the variance of simulated scores across each virtual population was calculated. From this distribution of simulated variances, 10,000 bootstrap replicates were taken and used to estimate confidence intervals and p-values of the null hypothesis test of no difference between the variance of the observed and the simulated preference scores.

Modeling of behavioral effects

Our goal was to measure the effect size of specific experimental manipulations on inter-fly odor preference variability. Isolating these effects is difficult for several reasons. First, observed behavioral variance is confounded by sampling error. To minimize the impact of sampling error, we could simply sample odor responses for a longer period of time; however, after several minutes, most flies adapt to the stimuli and behaviorally habituate. Second, manipulating environmental temperature and neural activity may produce changes in overall locomotor activity. Effects on some of these locomotor features are shown in Table S1. This issue directly impacts the sampling error issue, since less active animals will have fewer chances to cross the center and sample both odors, thus biasing preference scores toward extreme values (though, notably, the mean preference is unaffected [Fig S12]). Third, our measure of preference, a proportion, is bounded on $[0,1]$, which tends to artificially deflate estimates of dispersion. Indeed, variance is a poor measure of dispersion on bounded distributions because it is not robust to accumulated observations at the extrema. Furthermore, we believe that it is unlikely that two flies with a measured odor preference of e.g., 1, truly have the exact same magnitude of preference. Rather, our assay is incapable of resolving these differences because of sampling limitations, a phenomenon generally known as data censoring. These issues are further exacerbated when the mean is far from 0.5, causing more flies to accumulate at values of 0 or 1, thereby producing an artificial dependence of dispersion on the central tendency. Thus, we must be concerned that experimental manipulations which affect the mean can amplify the censoring effect and produce spurious apparent effects on variance. One possible way to address these concerns is to use non-parametric measure of dispersion, e.g., MAD or IQR, as done previously [10]. However, that only addresses the issue of measuring dispersion in a robust way. To address the other issues we must control for the confounding effects of overall locomotor activity on measured preference.

We used a linear modeling approach to address these challenges by jointly modeling the main effects of experimental manipulations, their interactions, and confounding “nuisance” parameters on both the mean and variance of odor preference scores. We developed a novel censored heteroscedastic

regression model, where experimental and environmental factors exert their effects on odor preference distribution independently and in combination. For example, preference variability in experiments utilizing thermogenetic reagents was potentially affected by two factors we would like to control for (genotype and experimental temperature) and by their interaction, which is the effect size we are actually interested in estimating [11]. The likelihood, L , of observing a particular odor preference, p_i , is calculated from a censored Normal distribution:

$$\mathcal{L}(p_i) = \mathcal{N}_{cens}(p_i, \mu_i, \sigma_i)$$

which assumes that the odor preference is a latent continuous variable and that observed values of 0 and 1 are really censored observations of preference values that extend beyond the observable range [0,1]. The formulation of odor preference as a censored latent variable makes the estimation of variance in the model insensitive to changes in the mean. The expected mean, μ , and standard deviation, σ , of odor preference for fly i :

$$\begin{aligned} \mu_i &= \mu_0 + \mu_{g_i} + \mu_{e_i} + \mu_{g_i * e_i} + f_{\mu}(\tau_i) \\ \sigma_i^2 &= \sigma_0^2 + \sigma_{g_i}^2 + \sigma_{e_i}^2 + \sigma_{g_i * e_i}^2 + f_{\sigma}(\tau_i) + \epsilon(d_i) \end{aligned}$$

depend on animal i 's genotype, environment, the interaction of genotype and environment (coded as binary indicator variables), and a term to account for seasonal effects of external air temperature (a scaled continuous variable). The standard deviation has an offset term, ϵ , defined for a given fly as:

$$\epsilon_i = a * dist_i^b + c$$

that depends on the distance, $dist$, traveled by fly i during the odor period and accounts for the increased uncertainty in estimating odor preference for inactive flies. The relationship between ϵ and $dist$ was determined empirically by fitting a function, of the form shown in Eq. 3, to the pre-odor variance-by-distance plot of a pilot dataset (Figure S1D). The coefficient values used in all three models were $a = 2.365$, $b = -0.651$, $c = -0.0077$.

As shown above, we included two nuisance terms in the model to adjust for uncontrolled sources of variability: an offset to the variance based on the distance traveled during the odor period, and an additional uncontrolled environmental variable (the average air temperature in Boston) that was observed to have a significant association with preference variability (Figure S7B,D). Air temperature data recorded at the Boston Logan International Airport weather station (WBAN:14739) were downloaded from the NOAA Climate Data Online website [11] for the time period encompassing our behavior experiments. Temperature values were scaled to have a mean of 0 and a standard deviation of 1. We suspect that outdoor air temperature is only a correlate of the true seasonal cause of

fluctuating variability, for which there are many possibilities including plant [12] or yeast [13] volatiles, or barometric pressure [14].

Bayesian model fitting

The model described above may be fit using maximum likelihood estimation or by using Markov Chain Monte Carlo (MCMC) simulation within a Bayesian framework. We chose to use the Bayesian approach, since the inclusion of reasonable prior expectations can provide parameter regularization and aid in model identifiability. Models were programmed in the Stan modeling language [15,16] and implemented using the RStan library [17] for R [18]. Model fitting was performed on the Odyssey cluster supported by the FAS Division of Science, Research Computing Group at Harvard University.

For each model, 32 MCMC chains were run in parallel using the No-U-Turn-Sampler implementation of the Hamiltonian Monte Carlo algorithm [19]. Briefly, 1,500 samples were drawn from each chain, and the first 1,000 warm-up samples were discarded. The remaining 500 samples from each chain were aggregated, for a total of 16,000 samples taken from the joint posterior. Several within-chain and between-chain diagnostic criteria were monitored for each model, in accordance with current best practices [20]. These diagnostics did not indicate any pathological MCMC behaviors for any of the models reported.

A series of pilot experiments using the control genotype (iso^{KH11}) under baseline conditions was used to update an initial set of vague priors on the mean intercept, variance intercept, and environmental air temperature coefficient terms in the model ($n = 3,722$ flies total). The posterior standard deviations (multiplied by a factor of ten to reflect more uncertainty) and means from this model were used as prior parameter values for their corresponding terms in subsequent models:

$$\begin{aligned}\mu_0 &\sim \mathcal{N}(0.5, 0.25) \\ \sigma_0^2 &\sim \mathcal{N}(0.012, 0.01) \\ f_\mu &\sim \mathcal{N}(-0.034, 0.03) \\ f_\sigma &\sim \mathcal{N}(-0.008, 0.01)\end{aligned}$$

For all regression coefficient priors, we used a Normal distribution, centered at 0, and selected weakly-informative, but reasonable, values for the scale:

$$\begin{aligned}\mu_g &\sim \mathcal{N}(0, 0.2) \\ \mu_e &\sim \mathcal{N}(0, 0.2) \\ \mu_{g*e} &\sim \mathcal{N}(0, 0.2) \\ \sigma_g^2 &\sim \mathcal{N}(0, 0.01) \\ \sigma_e^2 &\sim \mathcal{N}(0, 0.01) \\ \sigma_{g*e}^2 &\sim \mathcal{N}(0, 0.01)\end{aligned}$$

The overall goal for selecting priors was simply to provide some degree of regularization for parameter estimates and to aid in model identifiability, rather than to influence posterior estimates based on any prior expectations about specific effects. We fit a total of three separate regression models for: 1) neuromodulation experiments shown in Figures 3 and 5 (n = 5,327 flies total); 2) thermogenetic experiments using the *dTrpA1* effector in Figure 4 (n = 5,285); and 3) thermogenetic experiments using the *sh^{ts1}* effector in Figure 4 (n = 2,027).

Kernel Density Estimates (KDE) of odor preference distributions

The KDEs of odor preference were estimated in MATLAB using the KSDENSITY function with a Gaussian kernel. Kernel bandwidth was automatically chosen using the default optimal method for normal densities, and censoring was applied at values of 0 and 1, the upper and lower bounds of observable odor preference scores.

Measuring neurotransmitter concentration in fly head homogenates

The concentrations of serotonin and dopamine were measured in fly head homogenates using ELISA kits (Enzo Life Sciences Serotonin ELISA kit ADI-900-175) and (Abnova Dopamine ELISA kit KA1887). Flies spent 72 hours on drug supplemented food (α -MW, 5-HTP, or L-DOPA) or control food. Then flies were moved into an empty plastic vial (Genesee scientific 32-116) and placed in a -80C freezer to rapidly freeze, then heads were separated by forceps and pooled into groups of 10-15 heads in a 1.5mL microcentrifuge tube in 250uL of the kit ELISA assay buffer and homogenized using a pestle. The microcentrifuge tubes were spun down at 14,000rpm for 1 minute, and 2x 100uL of the supernatant was removed and placed into 2x microcentrifuge tubes to be used for the ELISA assay. The ELISA kit protocol, which include normalization steps for the number of loaded heads per sample, was then followed. All standards and samples were prepared in duplicate. The resultant plates were read at absorbance of 450nm (Dopamine ELISA) and 405nm (Serotonin ELISA). A standard curve was generated for both assays by applying a linear fit to the log concentration of the standards provided in each assay, with $r^2=0.91$ and $r^2=0.98$ for dopamine and serotonin standards respectively.

Supplementary Figures

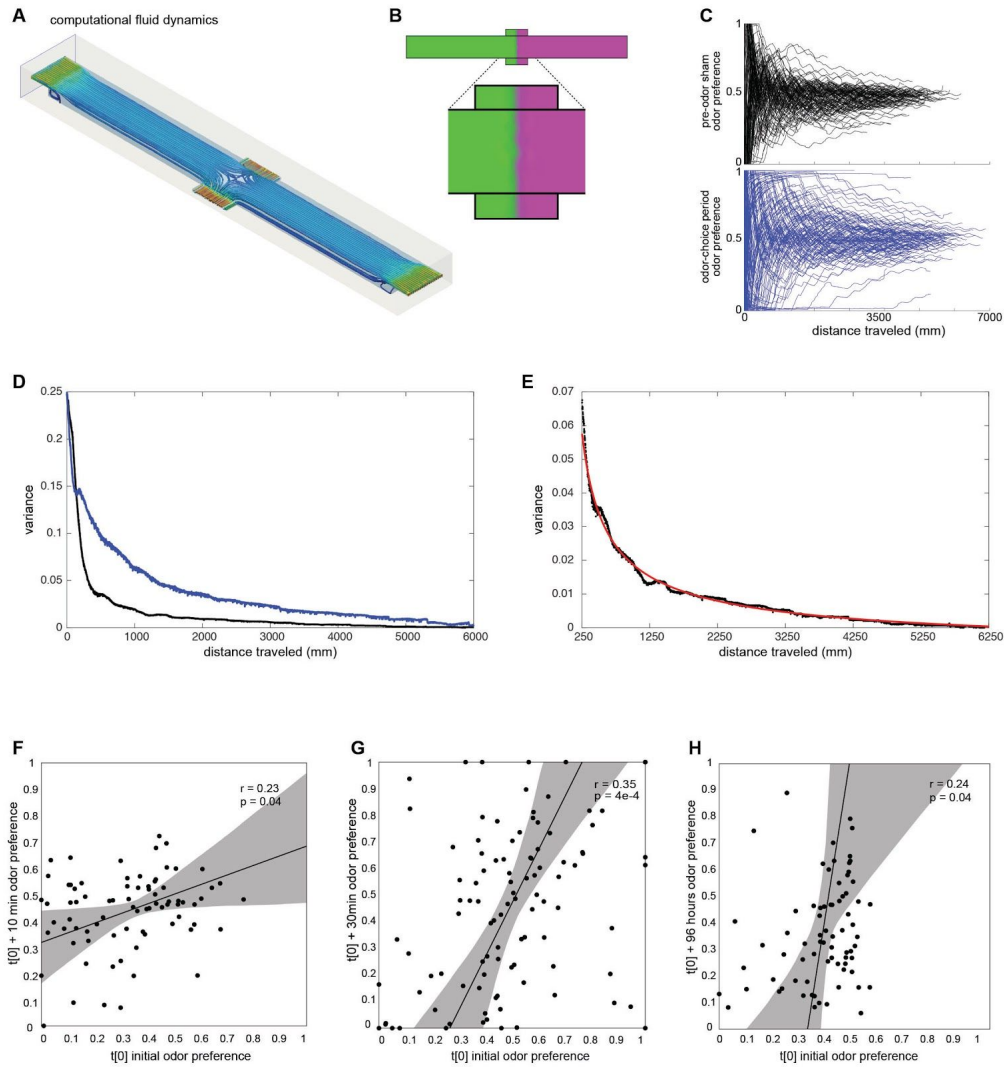


Figure S1 — Dynamics of odor stimuli and behavioral variability

- Computational Fluid Dynamics (CFD) simulation of steady state airflow through a single linear behavioral arena. Note the largely laminar flow along the length of the tunnel and the sharp flow boundary created in the center choice zone. Warmer colors indicate higher flow rates.
- CFD scalar mixing simulation showing the distribution of odor concentration at steady state. The scenario simulated the flow of an odorized stream (magenta) in one end of the arena (outlined in black) and clean air (green) in the other. A steep gradient is observed in the center choice zone, with little diffusion into the opposite arm.
- The running odor preference scores of 120 control (iso^{KH11}) flies as a function of distance traveled in the arena. Each line depicts the preference score trajectory of an individual fly. During the pre-odor period (top) most scores rapidly converge toward 0.5, but preference trajectories during the odor-choice period (bottom) are considerably more divergent.
- Across-fly variance of the trajectories depicted in S1C as a function of distance traveled. During the pre-odor period (black) variance rapidly converges toward 0 as most flies approach a preference of 0.5, but during the odor-choice period (blue) across-fly variance stays much higher as flies exhibit preference for an odor.
- Pre-odor period variance as a function of distance traveled (black) fitted by the function $\text{var} = 2.365 * \text{distance}^{-0.651} - 0.0077$ (red, $R^2 = 0.96$ for the region shown). This power-law relationship was used to calculate the activity-based variance offset for each fly.
- Correlation plot of individual fly odor preference 10 minutes after initial test versus during initial test. Pearson correlation $r = 0.23$, and $p = 0.04$. Line is the best fit as determined by minimizing orthogonal residuals using PCA (i.e., no explicit dependent or independent variables). Shaded area is the 95%CI of the regression line.
- As in F) except retested 3 hours later. Pearson correlation $r = 0.35$, and $p = 4e-4$.
- As in F) except retested 96 hours later. Pearson correlation $r = 0.24$, and $p = 0.04$.

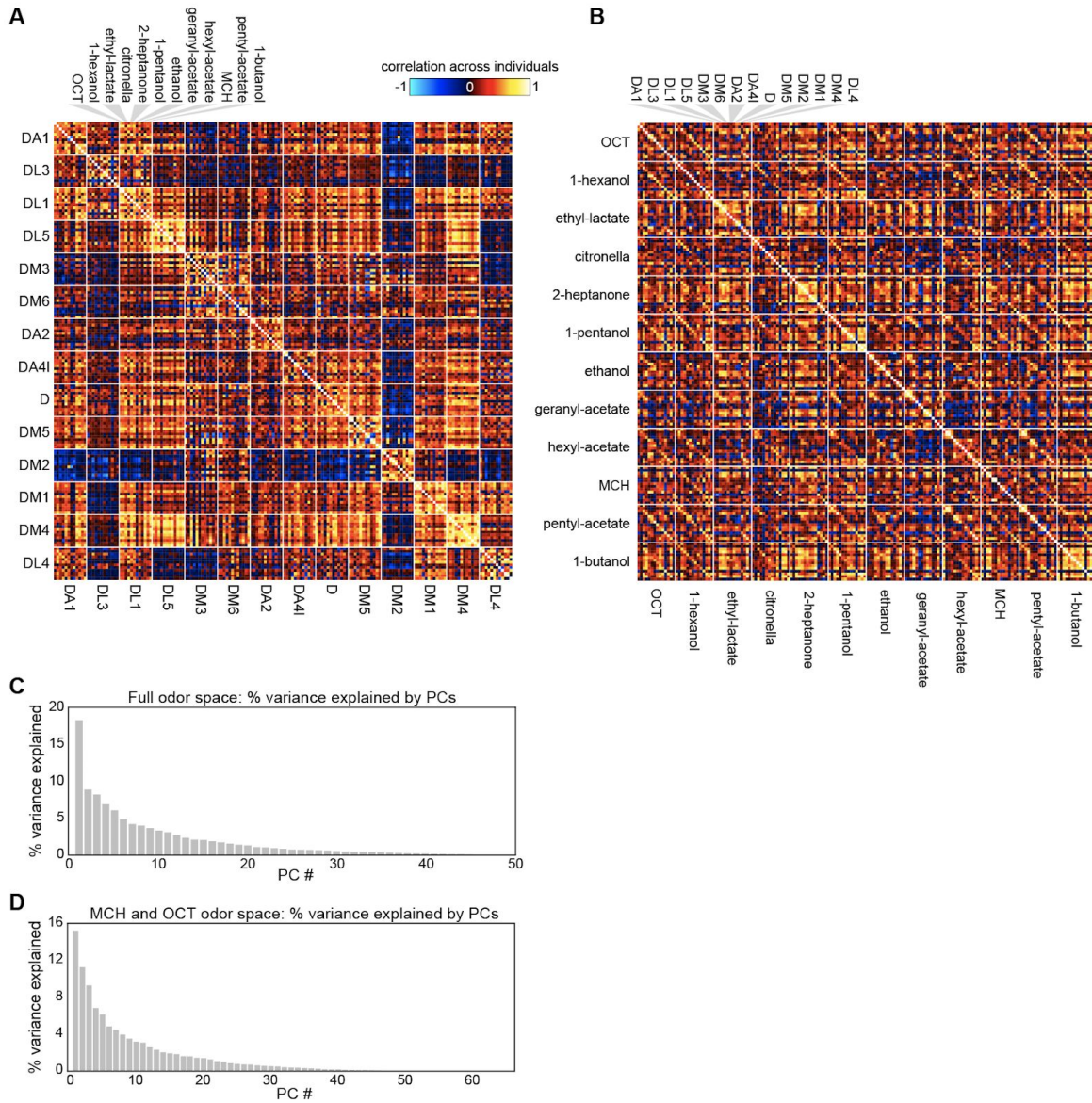


Figure S3 — Structure of odor response covariance.

A) Correlation matrix of Ca^{++} responses across individual flies. Rows and columns are organized by glomerulus and then odor. Here all responses for each odor are averaged within each fly. I.e., OCT and MCH values reflect the average of up to nine values (two values from the 12 odor panels, and the remainder from the OCT/MCH trials). The values for all other odorants are the average of the two responses per fly in the 12 odor panels.

B) As in A), except rows and columns are organized by odor and then glomerulus.

C) Ranked eigenvalues of the principle components of a Ca^{++} response space in which individual 12 odor panel trials are points and glomerulus-odor pairs are dimensions (corresponding to Figure 2I).

D) As in C) except for a Ca^{++} response space in which individual OCT or MCH trials are points and glomeruli are dimensions (corresponding to Figure 2J,K).

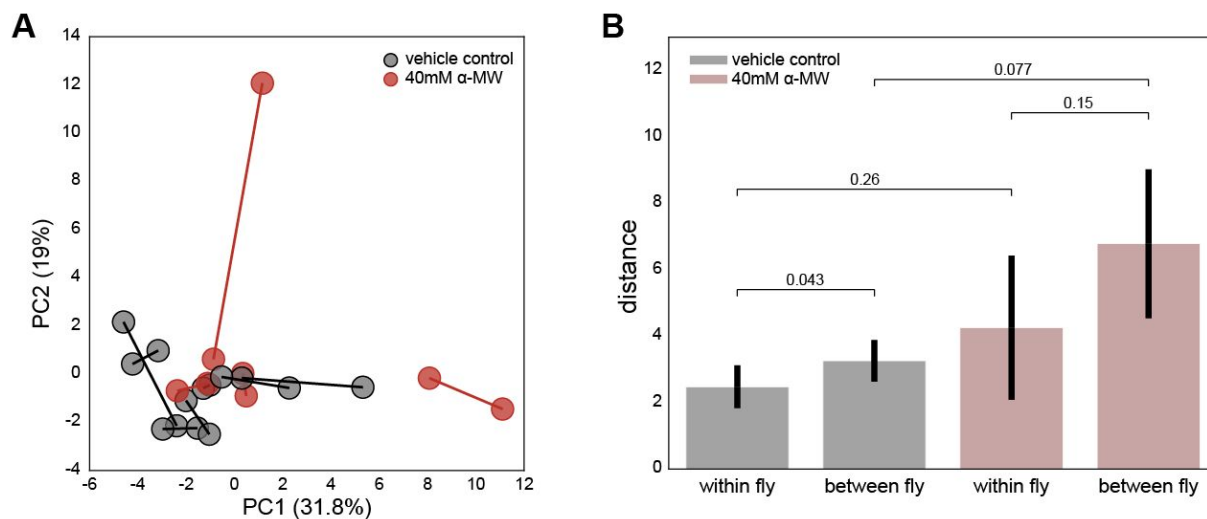


Figure S4 — PCA of odor responses in a data set with no missing values.

- A) PCA embedding of 12 odor panel trials for a data set with no missing values, i.e., the largest complete data set that can be made from the values in Figure S8 (containing 6 control flies and 4 α -MW-fed flies, with responses to two 12 odor panels across four glomeruli each. See Figure S8 and S9 for data from α -MW-feeding experiment). Projection onto PC1 and PC2 of the two 12 odor panel responses. Lines connect paired panels for each individual.
- B) Distance within and between flies in PC1-PC2 space for the data set used in A). Error bars are ± 1 standard error as determined by bootstrapping of individual flies. *P*-values within conditions reflect one-tailed resampling tests that the distance between flies is greater than the distance within. *P*-values between conditions reflect one-tailed resampling tests that α -MW distances are greater than control.

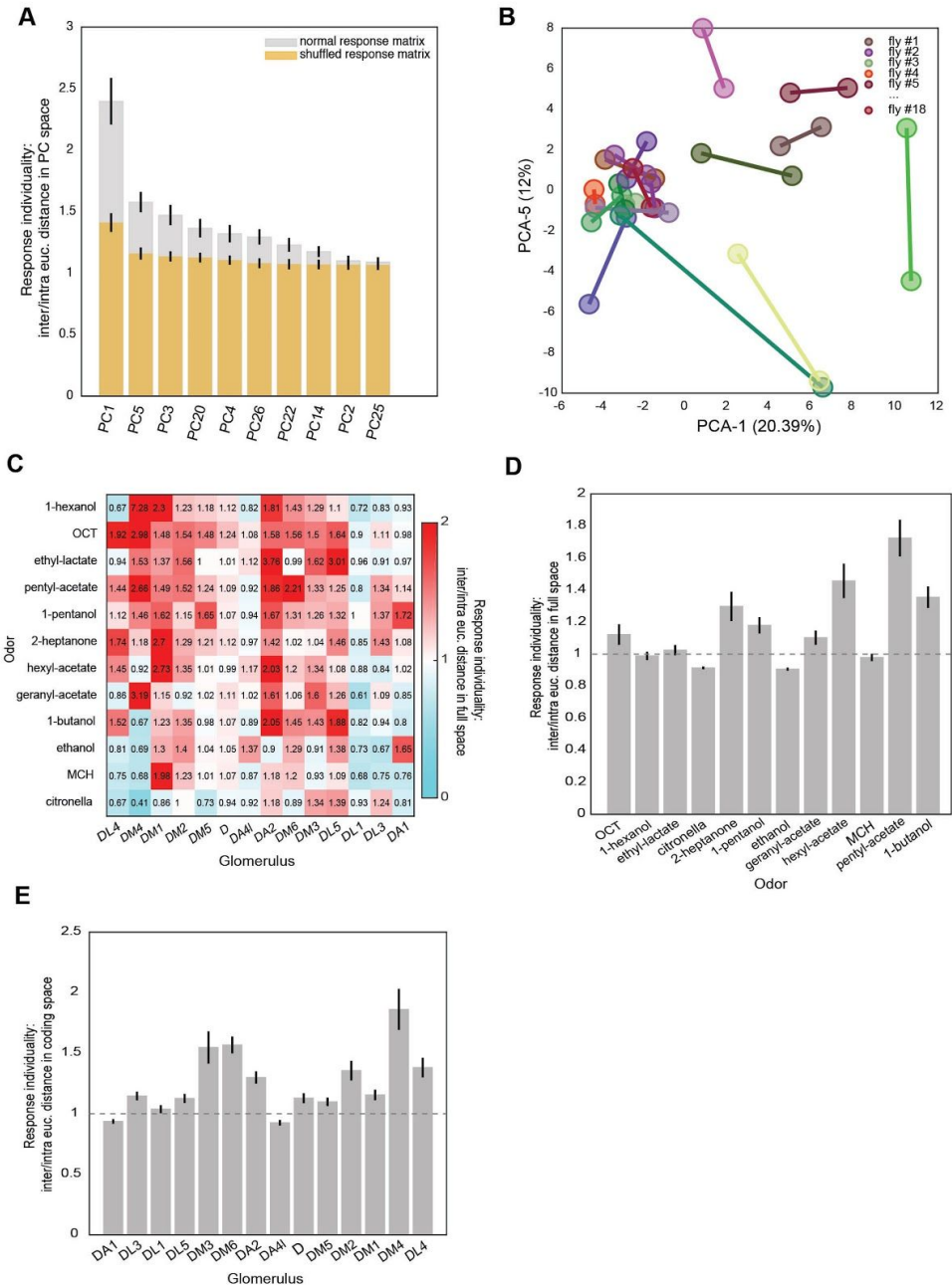


Figure S5 — Response individuality by odor and glomerulus.

- Individuality of odor responses on each principal component of response variation. Individuality was calculated by performing PCA on the original matrix of N-flies by 168 odor-glomerulus combinations. We then calculated inter-fly and intra-fly values using the same method as in Fig 2I), but only using a single indicated PC for each value.
- Scatter plot of odor panel responses on the two PCs with the highest individuality values, PC1 versus PC5.
- Matrix of individuality for each odor-glomerulus pair (i.e., each single dimension of the odor panel data set). Individuality was calculated by the ratio of inter-fly distance to intra-fly distance for each odor-glomerulus pair.
- Individuality by odor. Individuality was calculated by the inter-fly distance over intra-fly distance for all glomeruli responding to each odor as follows. For each odor, a response matrix of size 36 (18 flies, 2 trials each) X 14 glomerular responses was computed. Then the inter-fly distance and intra-fly distance was calculated using the same methods as in Figure 2I. Bars are +/-SEM calculated by 500-replicate bootstrap resampling of individuals.
- Individuality by glomerulus. Same as above in S5D), but estimating individuality of each glomerulus response across all 12 odors.

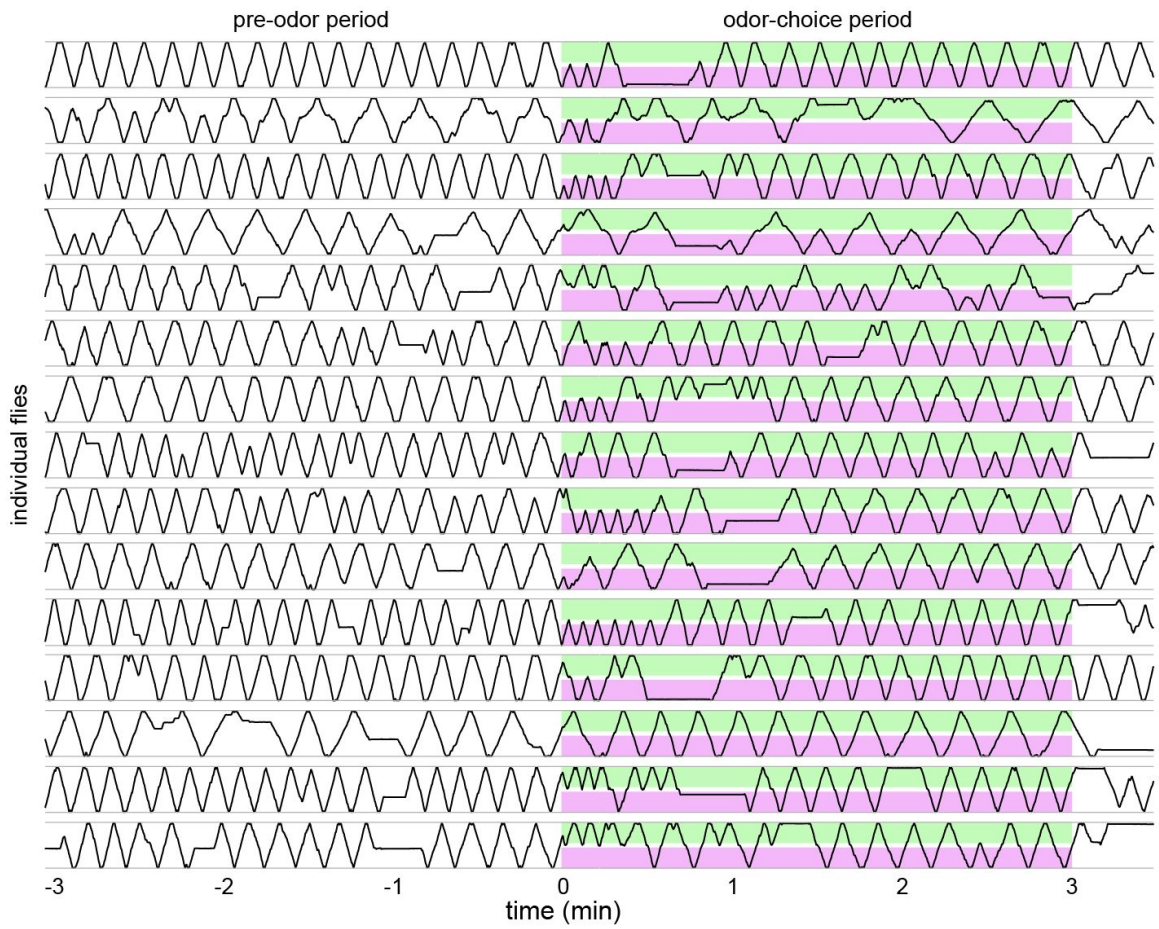


Figure S6 — Sample individual kymographs of odor behavior for *Dop1R1* flies. Reversals (turning around at the odor boundary) during the odor-choice period, indicate that the flies are detecting the odorants. Magenta = OCT, green = MCH.

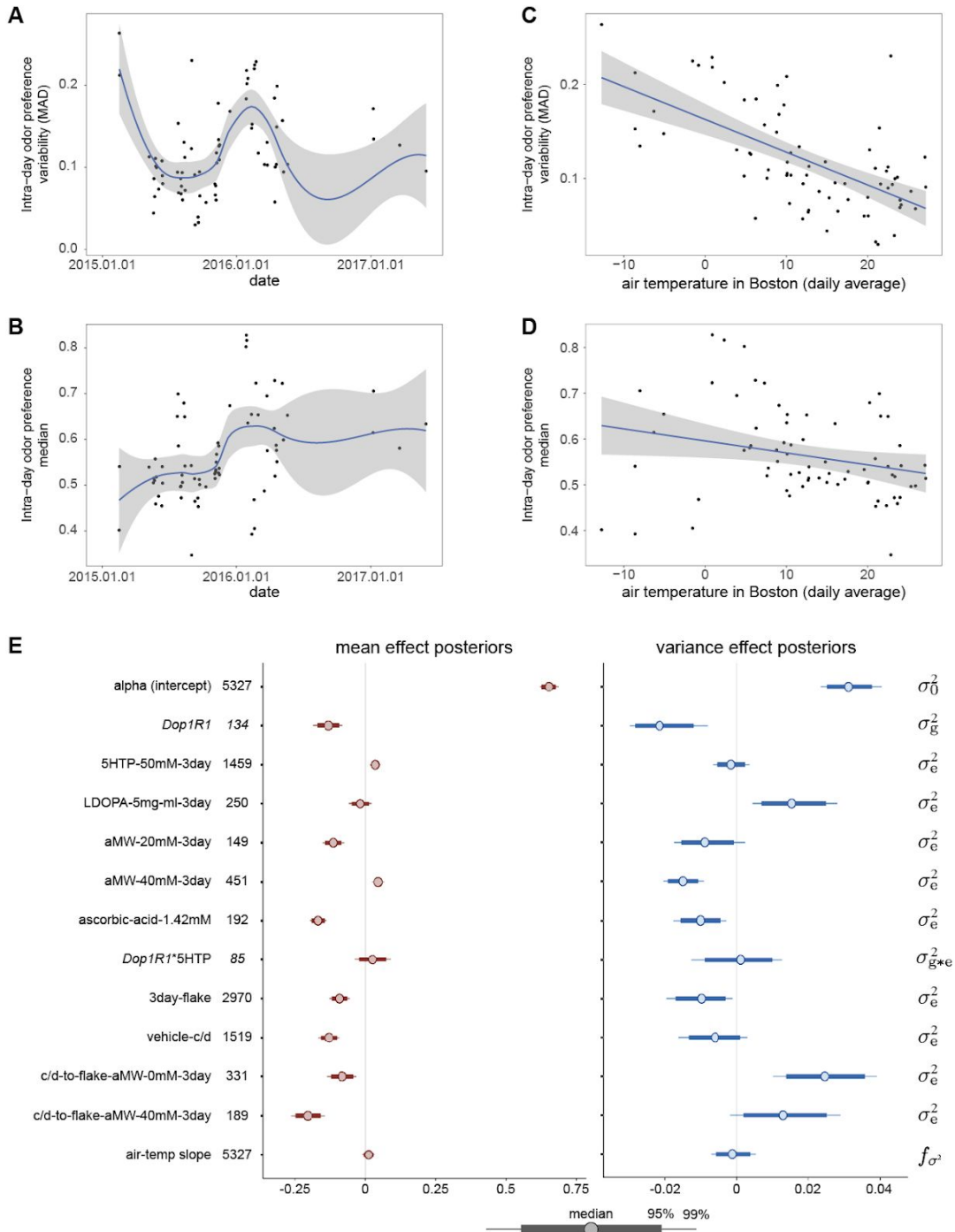


Figure S7 — Parameters of the Bayesian model of odor preference

- A) MAD (median absolute deviation) of wild type odor preferences measured daily (points) vs date. Blue line is a LOESS regression (span = 0.7), and grey region is the 95% CI. $n = 3722$.
- B) As in B) for the daily median of odor preference.
- C) MAD of wild type odor preferences measured daily (points) vs average daily temperature, as measured at the WBAN:14739 NOAA (Boston Logan International Airport) weather station. Blue line is a linear regression, and grey region is the 95% CI. $n = 3722$.
- D) As in D) for the daily median of odor preference.
- E) Forest plot of the posterior distributions for all parameters of the neuromodulation and food-shock model (Figures 3C and 5B). Labels at left indicate which type of coefficient each parameter is in the term for variability (σ^2). Numbers by parameter labels indicate the “marginal sample size,” i.e., the number of flies available to fit each parameter. c/d indicates cornmeal/dextrose media; flake indicates F4-24 food.

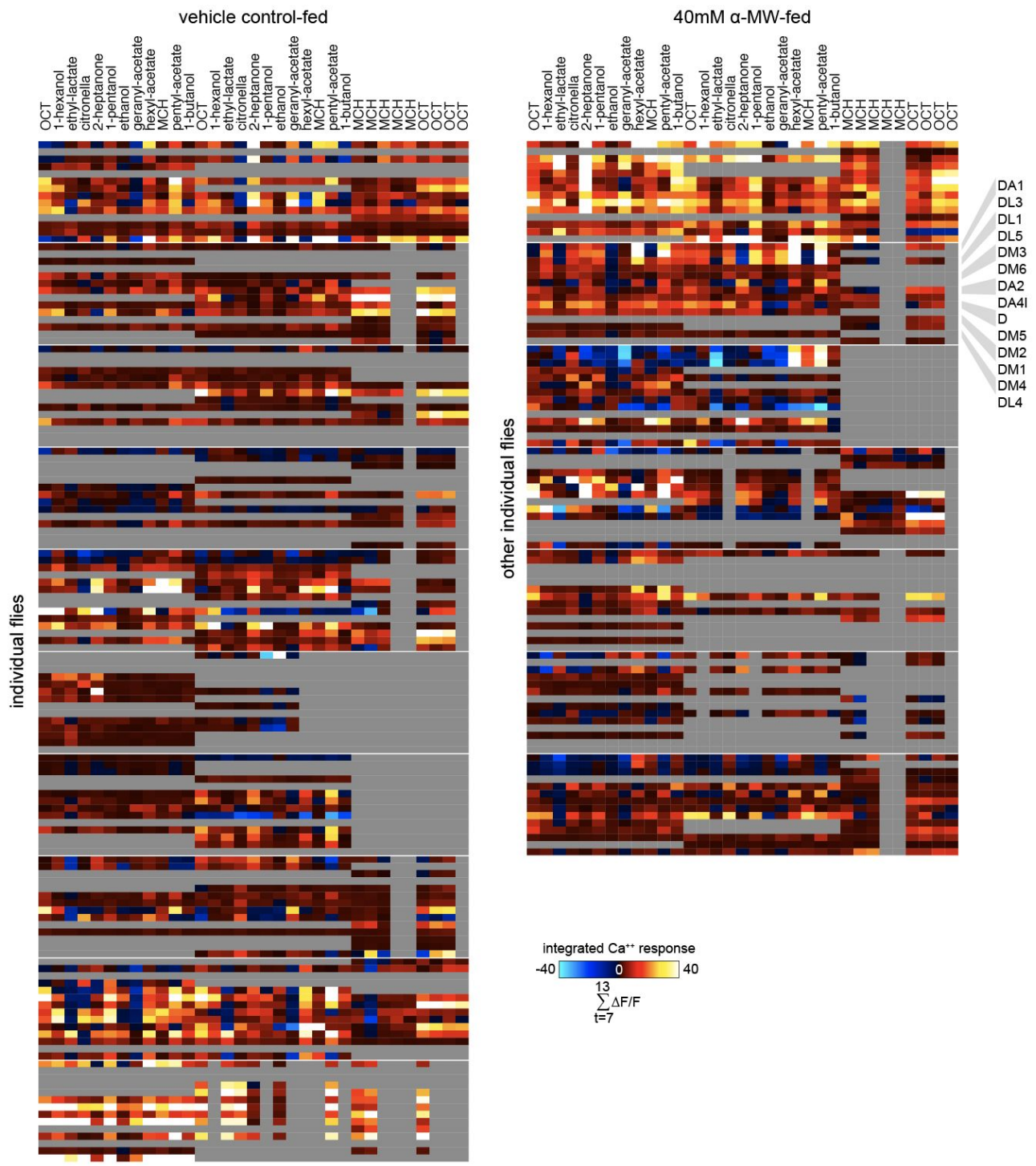
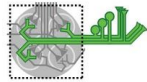


Figure S8 — Odor Ca^{2+} response matrices for control (left) and α -MW-fed (right) flies expressing GCaMP6m in GH146-Gal4 PNs. Integrated $\Delta F/F$ during and after the odor-stimulus period, by odor across the two 12 odor panels and OCT/MCH panel (columns). Rows are organized by individual fly and glomeruli.



PN dendritic Ca⁺⁺ responses (GH146>GCaMP6m)

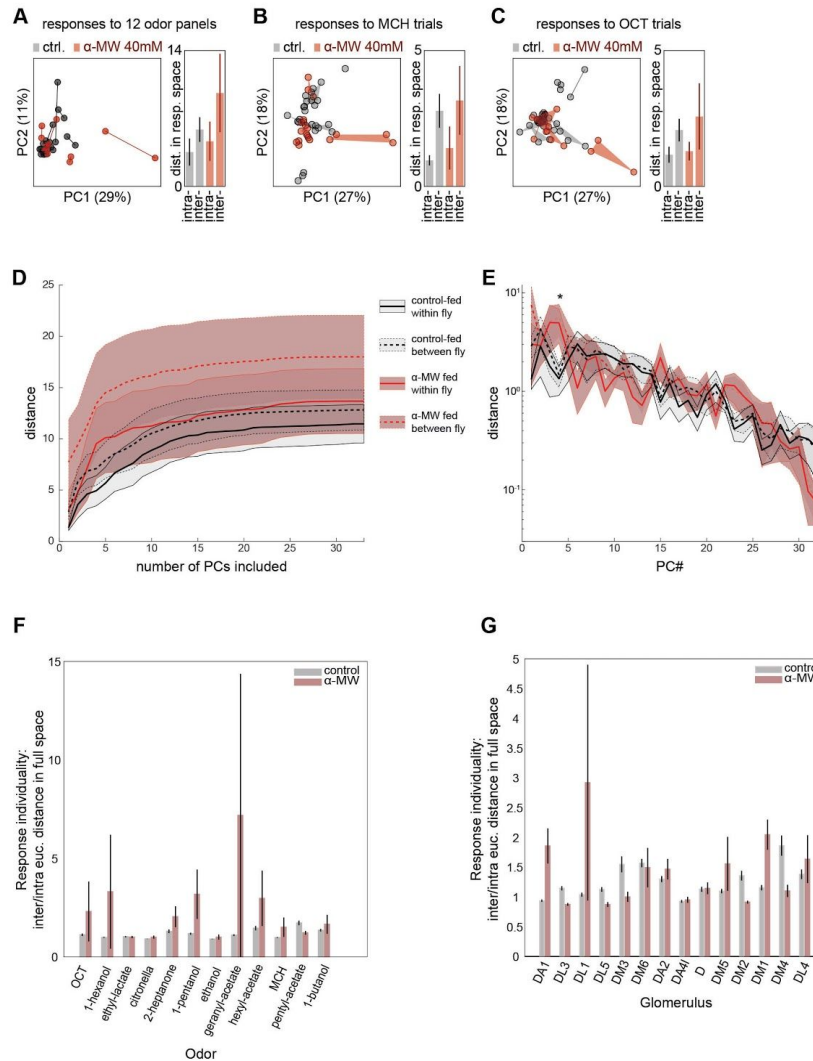


Figure S9 — PN dendrite Ca⁺⁺ responses in α -MW-fed flies and controls

- A) Left: Principal components 1 and 2 of individual panel responses in the space of odor-glomeruli responses (as in Figure 2I-K). Right: average distance among intra-fly trials and inter-fly trials. Bars indicate \pm SEM calculated by 20,000-replicate bootstrap resampling of individuals. The means within each treatment (intra- vs. inter-) are significantly different ($p=0.011$ and $p=0.024$) by one-tailed resampling. The means between treatments means are not statistically significant ($0.25 < p < 0.35$). Black indicates control flies, brown flies fed 40mM α -MW for three days.
- B) As in E) but with points representing responses to MCH in the 15 glomerular space containing MCH and OCT responses (as in Figure 2J and K). Intra- vs. inter- means are significantly different within control treatment ($p = 0.004$) but not statistically significant within α -MW treatment ($p = 0.093$). Differences in means between treatments means are not statistically significant ($0.34 < p < 0.40$).
- C) As in F) but with points representing responses to OCT in the 15 glomerular space containing MCH and OCT responses (as in Figure 2J and K). Means are significantly different within ($p < 0.001$) but not between ($0.34 < p < 0.39$) treatments.
- D) From the whole data set used in C, distance between control-fed and α -MW-fed trials as a function of the dimensionality of the projected PC space in which distances are calculated. Shaded areas represent \pm standard error as calculated by bootstrap resampling.
- E) As in F), but for distances (on a log y-axis) on just one PC at a time. α -MW-fed trials are significantly farther apart on PC4 than control trials (asterisk). $p = 0.028$ by bootstrapping based t-test comparing control and α -MW-fed inter-fly distances, and $p = 0.026$ for intra-fly distances.
- F) Individuality of Ca⁺⁺ responses for each odor, for control and α -MW treated flies. (See Figure S3.)
- G) Individuality of Ca⁺⁺ responses for each glomerulus, for control and α -MW treated flies. (See Figure S3.)

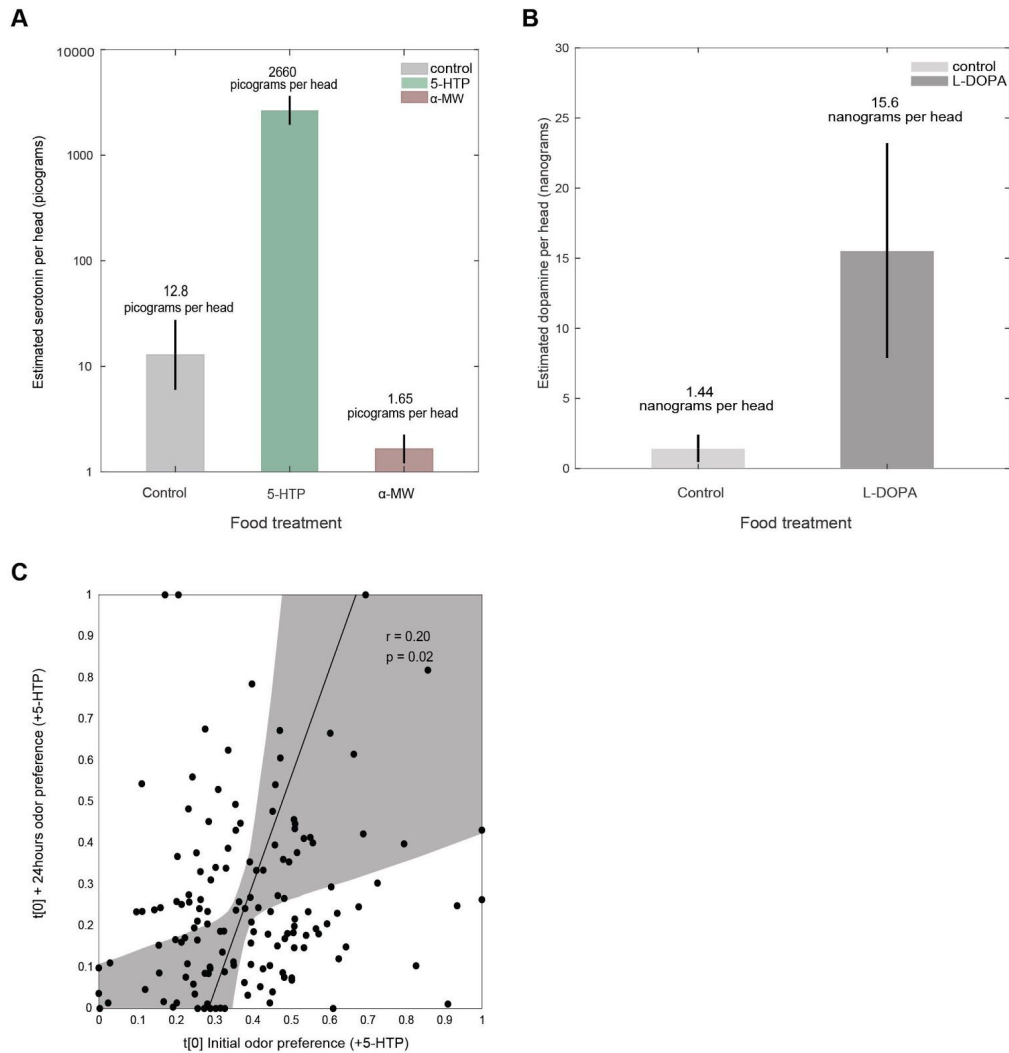


Figure S10 — Effects of 5-HTP, α -MW, and L-DOPA on neurotransmitter concentration in brain and day-to-day persistence of behavior.

- A) Estimation of the effect of α -MW and 5-HTP drug supplement on serotonin concentration per fly head via ELISA serotonin assay. For each assay, fly heads were pooled and homogenized to increase serotonin amounts to within the detectable range of the assay, as further described in the methods. Flies grown on control media yield an estimate of 12.8 picograms of serotonin per fly head. Flies grown on media supplemented with 5-HTP yield an estimate of 2660 picograms of serotonin per fly head. Flies grown on media supplemented with α -MW yield an estimate of 1.65 picograms of serotonin per fly head. We found that our estimate of serotonin per fly head after 5-HTP feeding is $\sim 10x$ larger than that reported by (Claridge-Chang et al., Cell 2009), as detected using HPLC. We believe our larger estimate is due to the cross-reaction of 5-HTP with the serotonin ELISA assay, which the assay manual reports. It is likely 0.4% of 5-HTP present in the samples was misidentified as serotonin.
- B) Same as in S8A) but for the effect of L-DOPA on dopamine concentration per fly head via ELISA dopamine assay.
- C) Correlation plot of individual fly odor preference 24 hours after initial test versus during initial test. Pearson correlation $r = 0.20$, and $p = 0.02$. Line is the best fit as determined by minimizing orthogonal residuals using PCA (i.e., no explicit dependent or independent variables). Shaded area is the 95%CI of the regression line.

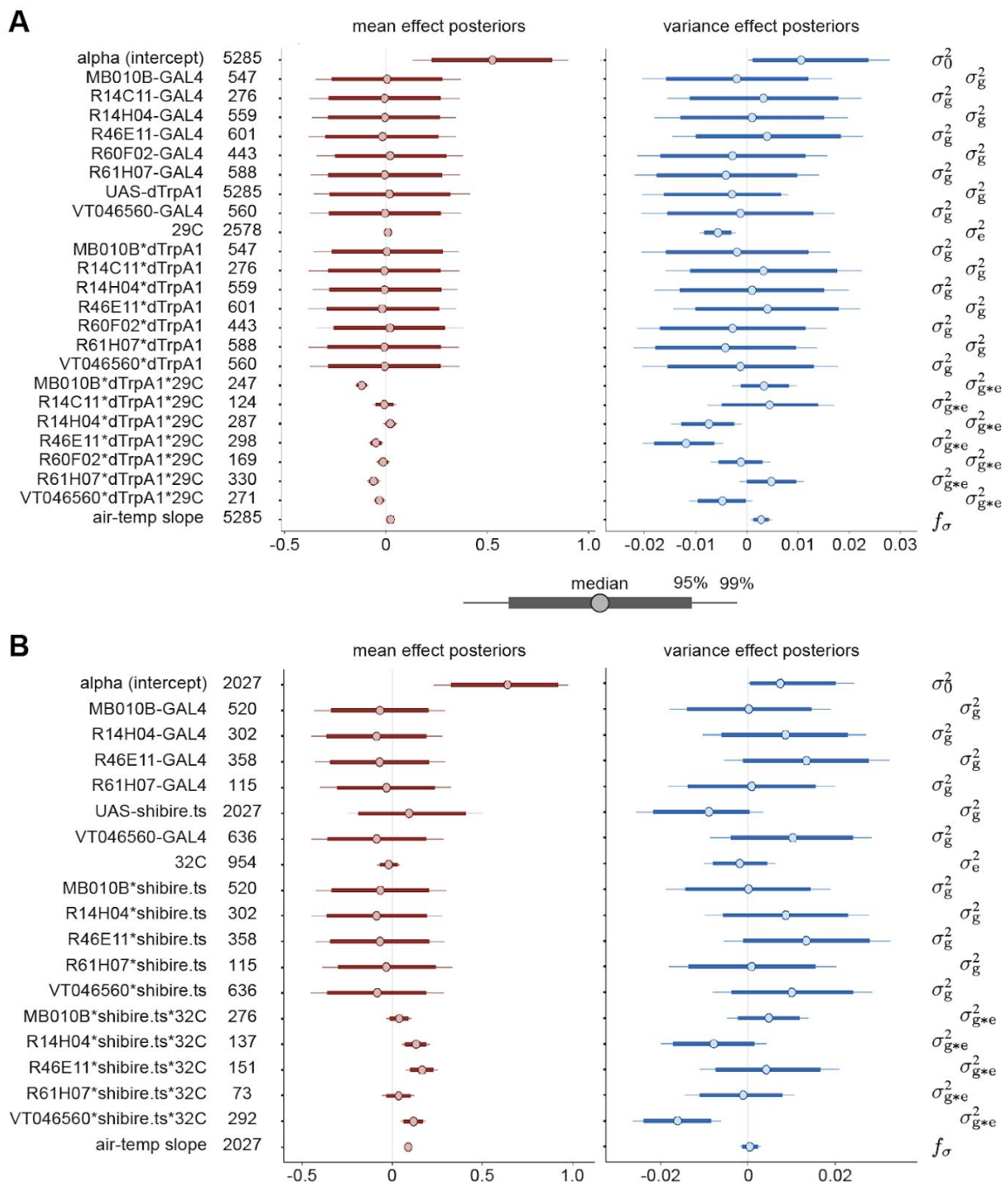


Figure S11 — Model parameters for thermogenetic experiments

- A) Forest plot of the posterior distributions for all parameters of the neural circuit dTRPA1 activation model (Figure 4D). Labels at left indicate which type of coefficient each parameter is in the term for variability (σ^2). Numbers by parameter labels indicate the “marginal sample size,” i.e., the number of flies available to fit each parameter.
- B) As in A), for Shibire^{ts} experiments.

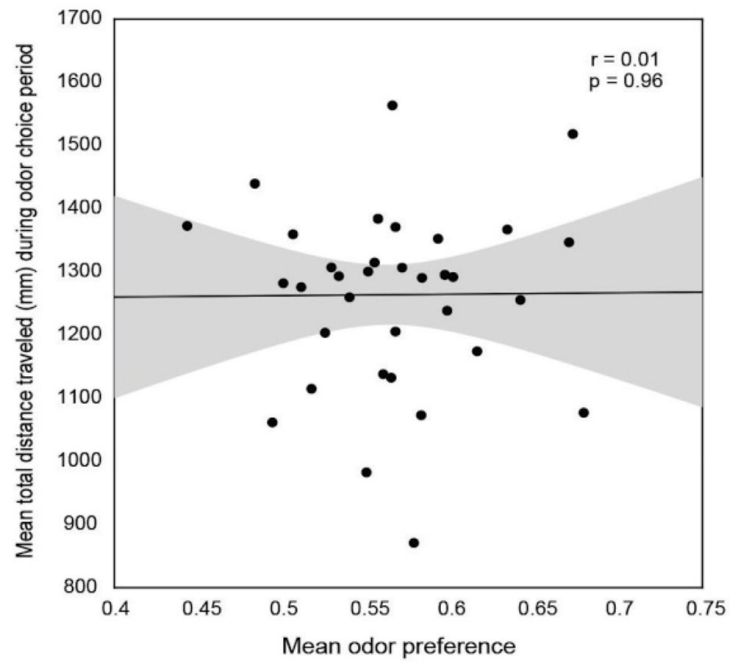


Figure S12 — Mean odor preference is independent of locomotor activity. Each point is the mean odor preference and mean total distance traveled within a single experimental factor (those listed in Figs S7 and S11). Factors estimated from fewer than 200 flies were excluded.

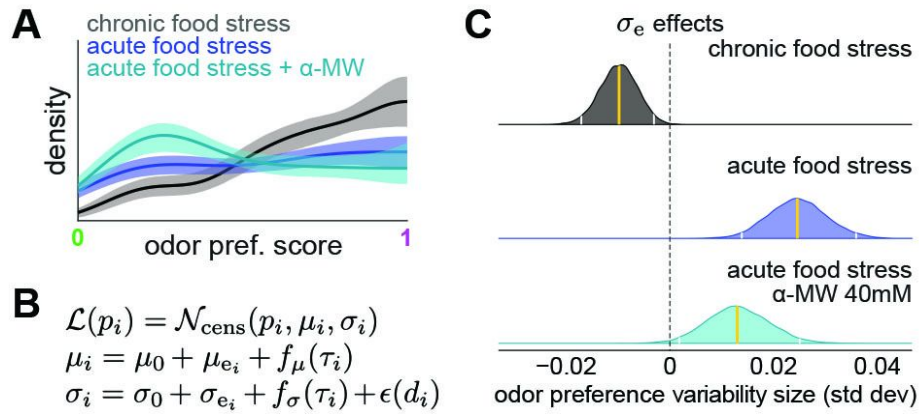


Figure S13 - Variability of odor preference is modulated by changes in diet

- Kernel-density estimates of the behavioral distribution of iso^{KH11} flies grown chronically on F4-24 flake food (gray), subject to a food stress treatment in which flies were transferred from cornmeal/dextrose food to F4-24 flake food (blue), and flies subject to the same food stress treatment but with 40mM α -MW in both food sources (teal). Shaded areas are 95% CIs.
- Model used to estimate the effects on odor preference variability of diet manipulations. Each term can be compared to those in Figs 3C and 4D.
- Posterior distributions of the effect of diet manipulations. Gold lines indicate the mean of the posterior, and white lines the edges of the 95% credible interval. Posterior distributions heavily overlapping 0 (dotted line) indicate no effect.

experimental group	n	pre-odor distance (mm)	odor-period distance (mm)	pre-odor reversals	odor-period reversals	pre-odor choice zone dwell (sec)	odor-period choice zone dwell (sec)
3day-flake	2970	1,357	1,132	1.23	7.40	0.97	1.34
5HTP-50mM-3day	1459	1,297	1,073	1.52	5.82	1.09	1.41
aMW-20mM-3day	149	1,543	1,379	1.51	7.98	0.95	1.02
aMW-40mM-3day	451	1,588	1,563	1.28	9.23	0.76	1.04
ascorbic-acid-1.42mM	192	1,464	2,143	1.22	10.32	0.78	1.01
Dop1R1	134	1,550	1,139	0.43	3.26	0.77	1.20
Dop1R1*5HTP	85	1,595	1,150	0.45	3.47	0.78	1.20
LDOPA-5mg-ml-3day	250	1,129	982	1.60	7.90	1.36	1.75
vehicle-c/d	1519	1,322	1,293	1.50	6.11	1.18	1.38
c/d-to-flake-aMW-0mM-3day	331	1,198	871	1.39	6.12	1.44	2.08
c/d-to-flake-aMW-40mM-3day	189	1,096	886	1.75	5.30	1.83	2.36
25C	1073	1,342	1,174	0.97	6.51	1.00	1.32
29C	2578	1,628	1,307	1.27	4.72	0.73	0.98
32C	954	1,398	1,347	1.54	5.30	1.70	1.26
MB010B-GAL4	1067	1,576	1,300	0.71	3.78	1.01	1.13
MB010B*dTrpA1	547	1,723	1,359	0.76	4.26	0.64	0.90
MB010B*dTrpA1*29C	247	1,673	1,373	0.69	2.58	0.60	0.75
MB010B*shibire.ts	520	1,422	1,238	0.65	3.29	1.41	1.38
MB010B*shibire.ts*32C	276	1,447	1,352	0.84	2.94	1.79	1.17
R14C11-GAL4	276	1,778	1,384	1.21	9.07	0.66	1.14
R14C11*dTrpA1	276	1,778	1,384	1.21	9.07	0.66	1.14
R14C11*dTrpA1*29C	124	1,883	1,474	1.64	8.36	0.66	0.99
R14H04-GAL4	861	1,457	1,307	1.07	6.04	1.06	1.08
R14H04*dTrpA1	559	1,520	1,315	0.92	5.85	0.72	1.01
R14H04*dTrpA1*29C	287	1,528	1,371	1.20	4.85	0.71	0.86
R14H04*shibire.ts	302	1,341	1,292	1.36	6.40	1.71	1.22
R14H04*shibire.ts*32C	137	1,314	1,377	1.64	4.95	2.52	1.31
R46E11-GAL4	959	1,365	1,205	1.40	6.34	1.19	1.22
R46E11*dTrpA1	601	1,506	1,282	1.11	6.05	0.82	1.08
R46E11*dTrpA1*29C	298	1,648	1,440	1.16	4.93	0.71	0.86
R46E11*shibire.ts	358	1,129	1,077	1.88	6.83	1.83	1.47
R46E11*shibire.ts*32C	151	931	979	2.68	5.95	3.06	1.79
R60F02-GAL4	443	1,894	1,295	0.77	6.01	0.83	1.10
R60F02*dTrpA1	443	1,894	1,295	0.77	6.01	0.83	1.10
R60F02*dTrpA1*29C	169	1,827	1,248	1.13	5.06	0.68	1.22
R61H07-GAL4	703	1,371	1,138	1.22	4.41	0.93	1.17
R61H07*dTrpA1	588	1,354	1,115	1.17	3.84	0.90	1.13
R61H07*dTrpA1*29C	330	1,185	1,062	1.72	3.06	1.04	1.12
R61H07*shibire.ts	115	1,457	1,257	1.46	7.35	1.11	1.36
R61H07*shibire.ts*32C	73	1,535	1,338	1.82	7.60	1.13	1.38
UAS-dTrpA1	5285	1,614	1,260	1.01	5.62	0.75	1.09
UAS-shibire.ts	2027	1,368	1,255	1.24	5.94	1.33	1.30
VT046560-GAL4	1196	1,507	1,290	1.38	6.08	0.83	1.16
VT046560*dTrpA1	560	1,565	1,204	1.48	5.16	0.74	1.15
VT046560*dTrpA1*29C	271	1,602	1,276	2.10	4.50	0.75	1.04
VT046560*shibire.ts	636	1,456	1,367	1.28	6.89	0.91	1.17

VT046560*shibire.ts*32C	292	1,590	1,518	1.45	6.66	0.79	1.06
-------------------------	-----	-------	-------	------	------	------	------

Table S1 — Mean values for various odor assay behavior features across experimental factors. The pre-odor and odor-period distances reflect the average total distance traveled (mm) by flies in each condition during the indicated experimental period. The number of reversals reflects the average number of turn around events during each experimental period. The choice zone dwell time (sec) reflects the average amount of time flies took to exit the choice zone after entering. Labels correspond to those in Figures S7 and S11.

Model parameters contributed to	Experimental group size
3d-carolina	1359
5HTP-50mM-3day; 3d-carolina	729
LDOPA-5mg_ml-3day; 3d-carolina	250
tan-to-carolina-aMW-0mM-3day	331
tan control	318
aMW-40mM-3day; ascorbic-acid-1.42mM; melted	102
ascorbic-acid-1.42mM; melted	90
5HTP-50mM-3day; melted	645
melted	682
aMW-20mM-3day; 3d-carolina	149
aMW-40mM-3day; 3d-carolina	349
dumb; 5HTP-50mM-3day; dumb*5HTP; 3d-carolina	85
dumb; 3d-carolina	49
tan-to-carolina-aMW-40mM-3day	189
UAS-dTrpA1	859
R46E11-GAL4; UAS-dTrpA1; R46E11*dTrpA1	303
R46E11-GAL4; UAS-dTrpA1; 29C; R46E11*dTrpA1; R46E11*dTrpA1*29C	298
UAS-dTrpA1; 29C	852
UAS-dTrpA1; VT046560-GAL4; VT046560*dTrpA1	289
UAS-dTrpA1; VT046560-GAL4; 29C; VT046560*dTrpA1; VT046560*dTrpA1*29C	271
R61H07-GAL4; UAS-dTrpA1; R61H07*dTrpA1	258
R61H07-GAL4; UAS-dTrpA1; 29C; R61H07*dTrpA1; R61H07*dTrpA1*29C	330
R14H04-GAL4; UAS-dTrpA1; R14H04*dTrpA1	272
R14H04-GAL4; UAS-dTrpA1; 29C; R14H04*dTrpA1; R14H04*dTrpA1*29C	287
R14C11-GAL4; UAS-dTrpA1; R14C11*dTrpA1	152
R14C11-GAL4; UAS-dTrpA1; 29C; R14C11*dTrpA1; R14C11*dTrpA1*29C	124
MB010B-GAL4; UAS-shibire.ts; 25C; MB010B*shibire.ts	244
MB010B-GAL4; UAS-shibire.ts; 32C; MB010B*shibire.ts; MB010B*shibire.ts*32C	276
MB010B-GAL4; UAS-dTrpA1; MB010B*dTrpA1	300
R60F02-GAL4; UAS-dTrpA1; R60F02*dTrpA1	274
MB010B-GAL4; UAS-dTrpA1; 29C; MB010B*dTrpA1; MB010B*dTrpA1*29C	247
R60F02-GAL4; UAS-dTrpA1; 29C; R60F02*dTrpA1; R60F02*dTrpA1*29C	169
UAS-shibire.ts; VT046560-GAL4; 25C; VT046560*shibire.ts	344
UAS-shibire.ts; 25C	71
R14H04-GAL4; UAS-shibire.ts; 25C; R14H04*shibire.ts	165

R46E11-GAL4; UAS-shibire.ts; 25C; R46E11*shibire.ts	207
UAS-shibire.ts; VT046560-GAL4; 32C; VT046560*shibire.ts; VT046560*shibire.ts*32C	292
UAS-shibire.ts; 32C	25
R14H04-GAL4; UAS-shibire.ts; 32C; R14H04*shibire.ts; R14H04*shibire.ts*32C	137
R46E11-GAL4; UAS-shibire.ts; 32C; R46E11*shibire.ts; R46E11*shibire.ts*32C	151
R61H07-GAL4; UAS-shibire.ts; 25C; R61H07*shibire.ts	42
R61H07-GAL4; UAS-shibire.ts; 32C; R61H07*shibire.ts; R61H07*shibire.ts*32C	73

Table S2 — By experimental group, the number of experimental flies contributing to different sets of model parameters. Adding up all the entries associated listing a particular parameter yields the “marginal sample sizes” listed in Figures S7 and S11.

Supplementary References

1. Yin JC, et al. (1994) Induction of a dominant negative CREB transgene specifically blocks long-term memory in *Drosophila*. *Cell* 79(1):49–58.
2. Brent MM, Oster II (1974) Nutritional substitution: a new approach to microbial control for *Drosophila* cultures. *Drosoph Inf Serv* 155:157.
3. Budick SA, Dickinson MH (2006) Free-flight responses of *Drosophila melanogaster* to attractive odors. *J Exp Biol* 209(Pt 15):3001–3017.
4. Honegger KS, Campbell RAA, Turner GC (2011) Cellular-resolution population imaging reveals robust sparse coding in the *Drosophila* mushroom body. *J Neurosci* 31(33):11772–11785.
5. Parnas D, Haghghi AP, Fetter RD, Kim SW, Goodman CS (2001) Regulation of postsynaptic structure and protein localization by the Rho-type guanine nucleotide exchange factor dPix. *Neuron* 32(3):415–424.
6. Lee T, Luo L (1999) Mosaic Analysis with a Repressible Cell Marker for Studies of Gene Function in Neuronal Morphogenesis. *Neuron* 22(3):451–461.
7. Hige T, Aso Y, Modi MN, Rubin GM, Turner GC (2015) Heterosynaptic Plasticity Underlies Aversive Olfactory Learning in *Drosophila*. *Neuron* 88(5):985–998.
8. Pologruto TA, Sabatini BL, Svoboda K (2003) ScanImage: flexible software for operating laser scanning microscopes. *Biomed Eng Online* 2:13.
9. Grabe V, et al. (2016) Elucidating the Neuronal Architecture of Olfactory Glomeruli in the *Drosophila* Antennal Lobe. *Cell Rep* 16(12):3401–3413.
10. Kain JS, Stokes C, de Bivort BL (2012) Phototactic personality in fruit flies and its suppression by serotonin and white. *Proc Natl Acad Sci* 109(48):19834–19839.
11. Nieuwenhuis S, Forstmann BU, Wagenmakers E-J (2011) Erroneous analyses of interactions in neuroscience: a problem of significance. *Nat Neurosci* 14(9):1105–1107.
12. Mansourian S, et al. (2018) Wild African *Drosophila melanogaster* Are Seasonal Specialists on Marula Fruit. *Curr Biol* 28(24):3960–3968.e3.
13. Becher PG, et al. (2012) Yeast, not fruit volatiles mediate *Drosophila melanogaster* attraction, oviposition and development. *Funct Ecol* 26(4):822–828.
14. Austin CJ, Guglielmo CG, Moehring AJ (2014) A direct test of the effects of changing atmospheric pressure on the mating behavior of *Drosophila melanogaster*. *Evol Ecol* 28(3):535–544.
15. Stan Development Team (2018) Stan User's Guide Version 2.18. https://mc-stan.org/docs/2_18/stan-users-guide/index.html

16. Carpenter B, et al. (2017) Stan: A probabilistic programming language. *J Stat Softw* 76(1). Available at: <https://www.osti.gov/biblio/1430202>.
17. Stan Development Team (2018) RStan: the R interface to Stan. R package version 2.18.2. <http://mc-stan.org/>.
18. R Core Team. (2019) R: A Language and Environment for Statistical Computing. *R Foundation for Statistical Computing*.
19. Hoffman MD, Gelman A (2014) The No-U-Turn sampler: adaptively setting path lengths in Hamiltonian Monte Carlo. *J Mach Learn Res* 15(1):1593–1623.
20. Gabry J, Simpson D, Vehtari A, Betancourt M, Gelman A (2019) Visualization in Bayesian workflow. *J R Stat Soc A* 182(2):389–402.